

THE SEQUENCE STRATIGRAPHY OF THE MIDDLE JURASSIC GYPSUM SPRING AND  
PIPER FORMATIONS IN THE EASTERN BIGHORN BASIN OF WYOMING, U.S.A.

by

ANNAKA M. CLEMENT

(Under the Direction of Steven M. Holland)

ABSTRACT

In northern Wyoming and southern Montana, the Aalenian–Bajocian Gypsum Spring and Piper formations preserve the earliest deposition in the Sundance Seaway. The facies and sequence stratigraphy of these formations were examined along the eastern flank of the Bighorn Basin, where they record deposition on a marine evaporite-carbonate ramp. Shallow-subtidal facies on this ramp pass landward into tidal flats, and then to mosaic of supratidal flats and marine-fed salinas. Three surfaces are recognized as sequence boundaries, the J-1a, J-1b, and J-2. The J-1a separates the lower and upper portions of the Gypsum Spring, and the J-1b separates the Gypsum Spring from the Piper. The position of the J-2 is resolved, separating the Piper from the Sundance Formation. The gypsum deposits of the Gypsum Spring are interpreted as basin-marginal evaporites based on facies association, and placed in the transgressive systems tract of the J-1 sequence.

INDEX WORDS: sequence stratigraphy, Middle Jurassic, evaporite, carbonate ramp, foreland basin, Sundance Seaway

THE SEQUENCE STRATIGRAPHY OF THE MIDDLE JURASSIC GYPSUM SPRING AND  
PIPER FORMATIONS IN THE EASTERN BIGHORN BASIN OF WYOMING, U.S.A.

by

ANNAKA M. CLEMENT

B.S., University of Wisconsin-Madison, 2013

A Thesis Submitted to the Graduate Faculty of The University of Georgia in Partial Fulfillment  
of the Requirements for the Degree

MASTER OF SCIENCE

ATHENS, GEORGIA

2015

© 2015

Annaka M. Clement

All Rights Reserved

THE SEQUENCE STRATIGRAPHY OF THE MIDDLE JURASSIC GYPSUM SPRING AND  
PIPER FORMATIONS IN THE EASTERN BIGHORN BASIN OF WYOMING, U.S.A.

by

ANNAKA M. CLEMENT

Major Professor: Steven M. Holland  
Committee: Bruce Railsback  
David Leigh

Electronic Version Approved:

Julie Coffield  
Interim Dean of the Graduate School  
The University of Georgia  
May 2015

## ACKNOWLEDGEMENTS

Thank you to Steve Holland for being an excellent advisor whose input and guidance on this project were indispensable. I am grateful also to Bruce Railsback and David Leigh for serving on my committee. Thanks to Kris Kusnerik for being my partner in crime. Many thanks to Kris Kusnerik, Jason Burwell, and Courtney Herbolsheimer for assistance in the field. My thanks as well to Cliff and Row Manuel for their assistance and hospitality in the field. Thank you to Daniel Graybeal, Jason Burwell, and Sydne Workman for the correlation of well logs in the study area and the surrounding area. Thanks as well to Corbin Kling and the UGA Center for Applied Isotope Studies for assistance with elemental analysis. Many thanks to Chelsea Jenkins, Pedro Monarrez, Silvia Danise, and C. Sean Cameron for their advice, conversations, and support throughout this project. My gratitude to my teachers, professors, and mentors both past and present for their invaluable lessons.

Thank you to the Geological Society of America, the Society for Sedimentary Geology (SEPM), and the Miriam Watts-Wheeler fund for generous funding of this project.

My thanks as well to my family (Carol, Jack, Emily, and Eleanor) and Andy for their constant love and support.

## TABLE OF CONTENTS

	Page
ACKNOWLEDGEMENTS .....	iv
LIST OF FIGURES .....	vi
CHAPTER	
1 INTRODUCTION AND LITERATURE REVIEW .....	1
2 THE SEQUENCE STRATIGRAPHY OF THE MIDDLE JURASSIC GYPSUM SPRING AND PIPER FORMATIONS IN THE EASTERN BIGHORN BASIN OF WYOMING, U.S.A. ....	3
<b>INTRODUCTION</b> .....	4
<b>GEOLOGIC SETTING</b> .....	5
<b>METHODS</b> .....	7
<b>FACIES</b> .....	10
<b>DISCUSSION</b> .....	23
<b>CONCLUSIONS</b> .....	35
CONCLUSION.....	37
REFERENCES .....	38
APPENDICES	
A COLUMN LOCATIONS.....	73
B ELEMENTAL ANALYSIS RAW DATA .....	74

## LIST OF FIGURES

	Page
Figure 1: Paleogeographic reconstruction of western North America in the Bajocian Stage (~170Ma) .....	47
Figure 2: Locations of Jurassic outcrop and measured sections in the eastern Bighorn Basin of Wyoming.....	49
Figure 3: Outcrop and thin section photographs of facies E1.....	51
Figure 4: Outcrop and thin section photographs of facies E2.....	53
Figure 5: Outcrop and thin section photographs of facies E3 and E4 .....	55
Figure 6: Outcrop and thin section photographs of facies E4, continued.....	57
Figure 7: X-ray diffraction of representative mudstones of the Gypsum Spring and Piper formations .....	59
Figure 8: Outcrop and thin section photographs of facies E5, E6, and E7 .....	61
Figure 9: Strontium to calcium ratios for columns where more than three gypsum beds were sampled .....	63
Figure 10: Principal components analysis of cation to calcium ratios from the lower gypsum beds of the Gypsum Spring Formation .....	65
Figure 11: Facies model showing interpreted lateral relationships among facies in the Gypsum Spring and Piper formations .....	67
Figure 12: Stratigraphic cross-section and sequence stratigraphic interpretation of the Gypsum Spring and Piper formations on the eastern margin of the Bighorn Basin .....	69

Figure 13: Revised chronostratigraphic chart for the Middle Jurassic of eastern Wyoming.....71

## CHAPTER 1

### INTRODUCTION AND LITERATURE REVIEW

This thesis has been prepared as a manuscript intended for submission to the journal *Facies*, and is therefore best read as a single chapter. The second chapter includes introduction, geologic setting, methods, facies association, sequence stratigraphic interpretation, discussion, and conclusion. The third chapter summarizes the conclusions. This project develops a facies model for an evaporite-carbonate ramp in Middle Jurassic rocks of north-central Wyoming, proposes a sequence stratigraphic interpretation of these rocks, and describes the sequence stratigraphic context of a widespread ancient evaporite deposit within these rocks.

The correlation and paleoenvironmental context of the Middle Jurassic strata in Wyoming have been of interest to geologists for over fifty years. Wilson (1955), Clifford (1963), and Greene (1970) made the earliest stratigraphic descriptions of the Gypsum Spring and Sundance Formations in north-central Wyoming. Around this same time, Imlay (1952) created correlation charts of Mesozoic strata for Wyoming and western North America. Pipiringos and O'Sullivan (1978) summarized the correlation of the Mesozoic units and named the regionally extensive unconformities (e.g. J-0). Brenner and Peterson (1994) defined the Mesozoic strata in terms of marine cycles, with cycles separated by these regionally extensive unconformities. This was expanded on by Kvale et al. (2001) by the addition of subcycles between the J-2 and J-3 unconformities. Parcell and Williams (2005) developed the first sequence stratigraphic interpretation that covered the northern and western Bighorn Basin in Wyoming and Montana. Regional facies changes in the Gypsum Spring Formation, documented by Doyle (1984), Meyer

(1984), and Guyer (1995), suggest that more regional facies models and sequence stratigraphic interpretation are required for the southern and eastern Bighorn Basin of Wyoming.

Widespread marine-evaporite deposits, such as the gypsum found in the Gypsum Spring Formation, are also of general interest. These deposits are common in the sedimentary record, and accumulated on a scale far larger than in modern settings (Kendall and Harwood 1996; Kendall 2010). This makes them difficult to place in a sequence stratigraphic context (Kendall 2010). Handford and Loucks (1993) proposed an idealized carbonate-evaporite-siliciclastic arid ramp model, which has evaporite deposition in the lowstand, transgressive, and highstand systems tracts. Understanding the environment of deposition and the distribution of evaporite deposits within a basin is integral to determining the sequence stratigraphic context of ancient evaporite deposits.

## CHAPTER 2

# THE SEQUENCE STRATIGRAPHY OF THE MIDDLE JURASSIC GYPSUM SPRING AND PIPER FORMATIONS IN THE EASTERN BIGHORN BASIN OF WYOMING, U.S.A.<sup>1</sup>

---

<sup>1</sup> Clement, A.C. and S.M. Holland. To be submitted to *Facies*.

## INTRODUCTION

Ancient widespread marine evaporite deposits are an important geologic feature for the minerals and petroleum industries, yet they do not form at the same scale anywhere in modern environments. Large evaporite deposits are most common near the end of the Paleozoic and in the middle to late Mesozoic, and these deposits essentially disappear from sedimentary record in North America after the Cretaceous (Peters 2006). The abundance of large evaporite deposits at these times in geologic history is almost certainly due to presence of large epicontinental seas, the presence of which are governed by plate tectonic motion (Railsback 1993). The largest evaporite deposits in the world (e.g. deposits in Zechstein, Williston-Elk Point, Michigan, Paradox, and Delaware basins) were deposited in intracratonic basins with epicontinental seas (Cauneanu et al. 2011). Given this control, evaporitic environments are impossible to reproduce at such a large scale today. For this reason characterization and context of these deposits must be studied in the sedimentary record.

A sequence stratigraphic approach allows evaporite deposits to be described in the context of a facies association and through a basin's history (Handford and Loucks 1993). Evaporites have been documented within every systems tract of sequence stratigraphy (Warren, 1989; Handford and Loucks 1993; Parcell and Williams 2005, Catuneanu et al. 2011). Their placement within systems tracts is often difficult because few studies have determined the facies relationships in ancient evaporite basins, and modern settings lack such extensive evaporite deposition (Doyle 1984; Railsback 1993; Guyer 1995; Parcell and Williams 2005; Peters 2006; Kendall 2010). Despite the difficulty, understanding the context of evaporite deposits within a systems tract is crucial because their placement allows for predictions about their distribution and association where direct observation is not possible (Catuneanu et al. 2011). This becomes

particularly important economically where evaporite deposits are a seal facies for a petroleum system such as the Ghawar field of the Arabian Gulf (Alsharhan and Kendall 1986).

The Middle Jurassic Gypsum Spring Formation of Wyoming is an extensive evaporite-bearing deposit and an ideal unit to study the facies association and distribution of evaporite deposits within a basin (Wilson 1955; Meyer 1984; Doyle 1984; Guyer 1995; Pipiringos and O'Sullivan 1978; Parcell and Williams 2005). The Gypsum Spring Formation and overlying Piper Formation have been described as recording either one or two transgressive/regressive cycles (Wilson 1955; Pipiringos and O'Sullivan 1978; Doyle 1984; Guyer 1995; Meyer 1984; Parcell and Williams 2005). A depositional model for facies relationships in the northwest part of the Bighorn Basin in Montana has also been proposed (Parcell and Williams 2005), but the Gypsum Spring Formation is widespread, and regional facies differences suggest a different facies model may be needed in the southeast part of the Bighorn Basin. Using a sequence stratigraphic approach, this project seeks to determine the origin of this large Jurassic evaporite-bearing unit along the eastern flank of the Bighorn Basin of Wyoming.

## **GEOLOGIC SETTING**

The Jurassic of western North America was a time of significant tectonic activity (Lawton 1994). A shift in plate motions along the convergent margin of western North America produced a back-arc extensional basin in the Early Jurassic. In the Middle Jurassic, arc magmatism moved eastward toward Nevada, and thrusting on its eastern side produced an epicontinental seaway in a retro-arc foreland basin across Wyoming, Montana, and Utah, and north into Canada. This seaway is called the Sundance Seaway (Fig. 1). Foredeep strata in the axis of the basin are not preserved, and this has led to criticism of this retro-arc foreland basin

interpretation (Lawton 1994; Parcell and Williams 2005). The basin has also been argued to represent a cratonic basin produced by shallow angle subduction (Lawton 1994). The Sundance Seaway filled with terrestrial deposits of the Morrison Formation by the Late Jurassic (Lawton 1994).

There is also no consensus on the amount of communication of the Sundance Seaway with the Pacific Ocean through the basin's western margin (Brenner and Peterson 1994; Lawton 1994; Parcell and Williams 2005; Blakey 2014). Some interpretations show a single narrow entranceway to the Sundance Seaway at approximately 50°N paleolatitude (Blakey 2014). Others depict a wider entrance with an island arc extending southward (Brenner and Peterson 1994; Lawton 1994; Parcell and Williams 2005).

Jurassic strata of Wyoming record at least four major marine transgressive cycles (Pipiringos and O'Sullivan 1978; Brenner and Peterson 1994; Parcell and William 2005). Marine withdrawal from the basin is marked by the regional J-1, J-2, J-3, J-4, and K-0 unconformities (Brenner and Peterson 1994; Kvale et al. 2001). Deposition of stratigraphic units occurred over a dynamic topography that included regional structural highs such as Belt Island and the Sheridan Arch (Brenner and Peterson 1994).

The Gypsum Spring Formation is the name given to the gypsum, red mudstone, and carbonate deposits between the Chugwater and Sundance formations in Wyoming. In northern Wyoming, it is divided into the Gypsum Spring and the overlying Piper formations (Imlay 1956; Pipiringos and O'Sullivan 1978; Imlay 1980; Brenner and Peterson 1994). The Gypsum Spring is exposed well along the margins of the Bighorn Basin in Wyoming, and it is commonly divided into lower, middle, and upper (Piper) subunits (Doyle 1984; Meyer 1984; Parcell and Williams 2005). The lower unit contains interbedded gypsum and red mudstone, the middle unit is

dominated by shallow marine carbonates, and the upper unit (Piper Formation) is red mudstone (Doyle 1984; Parcell and Williams 2005).

## **METHODS**

### *Field methods*

Thirteen stratigraphic columns were measured and described in the Bighorn Basin of Wyoming (Appendix A, Fig. 2). These form a ~147 km northwest to southeast transect along the eastern flank of the Bighorn Basin. The transect is oblique to depositional strike, with depositional dip to the northwest (Brenner and Peterson 1994; Parcell and Williams 2005; Blakey 2014). Two additional columns were measured in Cody and Thermopolis, Wyoming. Measured columns span from the Gypsum Spring Formation's contact with the underlying Chugwater Formation to the Piper Formation's (upper Gypsum Spring) contact with the overlying Sundance Formation. Column locations were selected based on quality of exposure and proximity to previously measured exposures of the Sundance Formation (McMullen et al. 2014). For each column, beds were described for lithology, thickness, ichnofossils, body fossils, carbonate grains, sorting, and physical sedimentary structures. Carbonate rocks are named using the Dunham (1962) classification. This was done to identify facies based on characteristic features formed in a depositional environment. Hand samples of carbonate facies were thin-sectioned and stained with alizarin red-S carbonate stain for additional facies characterization.

From these thirteen columns, a northwest to southeast cross section was constructed. Facies association and sequence stratigraphic architecture were interpreted along the cross-section.

### *X-ray diffraction analysis of mudstone*

Six hand samples of mudstone were collected for X-ray diffraction (XRD) analysis. Two samples each of red, green, and purple mudstone were collected to compare their mineral composition and aid in facies interpretation. Each sample was milled to a fine powder (approximately 10 microns) and placed in a powder mount for a bulk composition analysis by X-ray diffraction. Samples were scanned in 0.01 degree steps over a range of 2 to 80 degrees  $2-\Theta$  at a rate of 0.02 seconds per step by a Bruker D8-Advance XRD system.

### *Elemental analysis of gypsum*

Gypsum samples were collected for elemental analysis by inductively coupled plasma-optical emission spectroscopy (ICP-OES) to check for geochemical differences among gypsum facies. Gypsum samples were collected from six columns to test for compositional differences that can indicate different depositional environments. Similar compositions within a bed would indicate that the gypsum was deposited from a well-mixed brine, subaqueously, and highly variable composition would indicate a very shallow to subaerial depositional environment (Rosell et al. 1998). A change in the variability of the gypsum composition up a column or among sites would therefore shows a change in the environment of deposition for gypsum (Rosell et al. 1998).

A total of 56 samples were collected for elemental analysis. In five columns (Gypsum Spring Road North, Gypsum Spring Road, Trapper Creek, Sheep Mountain, Sheep Mountain South, and Hyattville Alkali Road), one sample from each gypsum bed was collected. Two of these columns were widely spaced (Trapper Creek and Hyattville Alkali Road), and two pairs of columns were closely spaced (Gypsum Spring Road North and Gypsum Spring Road as well as

Sheep Mountain and Sheep Mountain South). Widely spaced columns were greater than two kilometers apart, and closely spaced columns were less than two kilometers apart. These samples were collected to check for changes in gypsum composition up section and for variability among sites.

In two columns (Sheep Mountain South and Hyattville Alkali Road), replicate samples were taken from two beds in each column. Six replicate samples, spaced one meter apart, were taken from two beds in each column to test for variability in composition within a bed. Sheep Mountain South and Hyattville Alkali Road were selected for replicate samples based on the quality of exposure and number of distinct gypsum beds.

All gypsum samples were hand-ground, treated for 40 minutes with 10% HCl to remove any carbonate, and dissolved in deionized water for ICP-OES analysis. Dissolved samples underwent twenty-element ICP-OES by a Perkin Elmer Optima 8300 Inductively Coupled Argon Plasma analyzer at the University of Georgia Center for Applied Isotope Studies. The twenty-element analysis included Al, B, Ba, Ca, Cd, Co, Cr, Cu, Fe, K, Mg, Mn, Mo, Na, Ni, P, Pb, Si, Sr, and Zn.

Comparison of elemental analysis results and principal components analysis (PCA) was carried out to differentiate any gypsum facies. Statistical analyses were performed in R (R Core Team 2013). Before statistical analysis, the amount of sodium was corrected by subtracting the sodium value from the digest blank from all samples, and elemental values below their detection limits were converted to zero. Elemental values were divided by the amount of calcium in each sample to produce a cation to calcium ratio, allowing elemental proportions to be easily compared to one another. Columns of constants (including zero) were culled from the analysis. A

principal components analysis was performed on the ratios to determine the primary sources of variation in the data to aid in identification gypsum facies.

## FACIES

Seven facies are recognized here from the Gypsum Spring and Piper formations.

### *Facies E1: peloidal to skeletal wackestone to packstone*

**Description**—Facies E1 is lithologically variable and includes argillaceous lime mudstone, lime mudstone, skeletal wackestone, peloidal packstone, and skeletal packstone (Fig. 3a, b). These lithologies are frequently interbedded with one another (Fig. 3a, b). Argillaceous lime mudstone is gray, contains frequent argillaceous partings, and its bedding is wavy and very thin. Argillaceous lime mudstone occasionally contains thin beds of lime mudstone with wavy, possibly microbial, lamination and rare bivalve fragments.

Gray lime mudstone is very thin to medium bedded with wavy, possibly microbial, lamination and contain rare fragments of bivalves and ostracods (Fig. 3c). Lime mudstone beds are resistant to weathering and often form ledges on hogbacks.

Skeletal wackestone is gray and very thin to thinly bedded (Fig. 3d). Skeletal fragments include oysters, bivalves, and ostracods. Skeletal grains are generally fragmented, but are occasionally whole and well-preserved.

Peloidal packstone beds display a clotted texture of peloids (Fig. 3e). They are very thin to medium bedded and often contain wavy lamination. Peloids are well sorted, abundant, and fine to very fine sand sized. Rare ostracods and quartz silt grains are also present.

Skeletal packstone is present only in the northernmost two columns, Gypsum Spring Road North and Gypsum Spring Road (Fig. 3f). It is very thinly bedded, and contains abundant bivalves, common echinoderms and ostracods, and rare oysters. Quartz silt is also present.

The thickness of facies E1 is 0.5–6 m, and it thickens and becomes more fossiliferous to the north. Facies E1 always has a sharp basal contact wherever the facies was observed. Facies E1 grades upwards into facies E3 and E4.

**Interpretation**—Facies E1 is interpreted to have been deposited in an open-marine setting on the shallow-subtidal part of a carbonate ramp. The skeletal grains in all the lithologies are of marine taxa (Lees and Buller 1972; Flügel 2010). The amount of skeletal material increases basinward (northward), with skeletal wackestone and packstone representing increasingly distal shallow-subtidal settings (Lees and Buller 1972; Lees 1975; Carozzi 1989; Bachmann and Kuss 1998; Bachmann and Hirsch 2006; Flügel 2010). The most distal lithology, skeletal packstone, is present only in the northernmost two columns (Gypsum Spring Road North and Gypsum Spring Road).

Lime mudstone and peloidal packstone are typical of relatively proximal open shallow-subtidal facies (Lees and Buller 1972; Lees 1975; Carozzi 1989; Bachmann and Hirsch 2006; Flügel 2010). On extratropical and cooler-water ramps, peloids are found in areas of higher salinity, suggesting some restriction on proximal areas of the ramp (Lees and Buller 1972; Lees 1975). The lime mudstone in facies E1 could have multiple sources, including disintegration of skeletal fragments or calcareous algae (Lees and Buller 1972). Calcareous algae is more common in tropical carbonate shelf settings, but a higher salinity can compensate for a lower water temperature and allow calcareous algae growth (Lees and Buller 1972; Lees 1975). This also suggests some restriction in more proximal areas of the ramp.

### *Facies E2: ooid grainstone*

**Description**—The ooid facies consists of very thin to thinly bedded ooid grainstone (Fig. 4). The ooids are medium lower to fine lower sand sized, and they contain a variety of cores, including quartz silt, skeletal grains, chert, sparry calcite, micrite, and an unidentified hexagonal mineral (Fig. 4c, d). Some cores are partially or completely micritized while others remain cortoids. The skeletal grains in ooid centers include bivalve fragments and whole gastropods. The outer portion of the ooids is a combination of radial crystalline calcite and micritic concentric lamellae (Fig. 4c, d, e). Calcite cement incompletely fills pore space between the ooids (Fig. 4c, d), and at Gypsum Spring Road, pore space is filled with recrystallized gypsum (Fig. 4e). The grainstone also contains peloids, intraclasts of micrite, and extraclasts of chert. Some samples contain recrystallized grains of partially rehydrated anhydrite with inclusions of anhydrite and calcite (Fig. 4e). Many ooids are broken or cross-cut one another, indicating some amount of pressure dissolution; however, stylolites were not observed (Fig. 4d, e). At Trapper Creek, the ooid grainstone has fine lower to very fine upper sand grains size, has little evidence of pressure dissolution, and contains uncoated skeletal grains and peloids (Fig. 4f).

Beds of ooid grainstone are separated by brown-gray mudstone or lime mudstone. Beds of ooid grainstone are laterally discontinuous (Fig. 4b), and a single bed cannot be traced more than ~40 m. Ooid grainstone beds lack lamination or cross-lamination. The base of facies E2 is always sharp, and facies E2 is gradationally overlain by facies E1.

**Interpretation**—Facies E2 is interpreted to have been deposited adjacent to an ooid shoal. The ooid grainstone beds in the Gypsum Spring Formation are thin and not cross-laminated or cross-bedded, indicating that these beds were not deposited within the shoal itself (Read 1985). The lack of lamination suggests extensive bioturbation (Droser and Bottjer 1993).

The heterogeneity of ooid cores, particularly chert and quartz grains, as well as the presence of chert extraclasts indicates a siliciclastic source of sediment (Flügel 2010). Ooid beds are laterally discontinuous, suggesting limited ooid production in the study area, and possibly that the ooids were transported from nearby shoals that were not encountered in the study (Simone 1980).

Ooid grainstone beds contain micritic layered or concentric ooids that form in high-energy environments. The same ooid grainstone beds also contain crystalline layered or radial ooids, which form in low-energy environments (Simone 1980; Flügel 2010). The presence of both concentric and radial ooids together suggests the ooids were transported from their original environments of production. Many ooids are broken, which is also evidence of transport (Flügel 2010).

Ooid formation is dependent on temperature and salinity (Lees and Buller 1972; Lees 1975). Ooids typically form in tropical warm-water settings or in waters with high salinity. They therefore frequently form in shoals seaward of lagoons where high salinity water mixes with more normal marine water, such as in the Persian Gulf (Lees and Buller 1972; Lees 1975; Simone 1980; Pierre et al. 2010). Fringing shoals have also been described in environments like Shark Bay, Australia where ooid production is immediately seaward of intertidal facies. In these cases, a shallow platform produces the necessary elevated temperature and salinity (Read 1985).

These examples give two possibilities for the environment of deposition for the ooid grainstone beds. Ooids in the Gypsum Spring may be a distal part of a shoal complex that is more basinward (north) of the study area; the thin ooid beds would represent distal portions of a more developed shoal. In contrast, the ooid beds may be part of a fringing shoal depositionally updip or potentially along depositional strike of shallow-subtidal environments. If produced in a fringing shoal environment, the lateral discontinuity and thinness of the ooid grainstone beds

may indicate that the conditions for ooid production were patchy and short-lived and thus did not produce the thick cross-bedded deposits commonly associated with this facies (Read 1985).

The sharp base of facies E2 indicates that the relationship between E2 and any underlying facies is non-Waltherian. That facies E2 is overlain with skeletal packstone from facies E1 favors the interpretations that these beds formed distally to an ooid shoal setting.

*Facies E3: laminated red and gray lime mudstone*

**Description**—Facies E3 contains very thinly laminated to very thinly bedded light gray, mottled red and gray, and red lime mudstone to skeletal wackestone (Fig. 5a, b). Light gray lime mudstone contains thin planar to sub-planar laminations, often with limonite and glauconite, as well as abundant moldic bivalves (Fig. 5c). The bivalves are nearly monospecific, consisting primarily of *Pleuromya*. Skeletal fragments are also concentrated along laminae to form a wackestone. Light gray lime mudstone and wackestone grade vertically into mottled red and gray lime mudstone. Mottled lime mudstone is very thinly laminated to very thinly bedded and contains abundant moldic bivalves along some laminae, although they are less abundant than in the gray lime mudstone. Mottled lime mudstone grades vertically into red lime mudstone. Red lime mudstone is very thinly laminated to very thinly bedded and contains rare moldic bivalves and skeletal fragments.

Each column contains one to three cycles of facies E3. A complete cycle begins with light gray lime mudstone that grades vertically into mottled gray and red lime mudstone and finally into red lime mudstone. The basal contact of each cycle is sharp, and these cycles cannot be correlated among columns.

Facies E3 is 2–5 m thick. Facies E3 gradationally overlies facies E1 and passes gradationally upward into facies E4.

**Interpretation**—Facies E3 is interpreted to have been deposited in a restricted marine shallow-subtidal ramp environment. The fossil assemblage, consisting mostly of bivalves, in facies E3 is marine (Less and Buller 1972; Lees 1975), but the high abundance and low diversity suggests a restricted shallow-subtidal environment of deposition (Flügel 2010).

The lithology, scarcity of skeletal grains, and fine lamination in facies E3 also indicate a restricted environment (Less and Buller 1972; Lees 1975; Flügel 2010). Lime mudstone is frequently produced from calcareous algae (Less and Buller 1972), and on non-tropical carbonate ramps without coral reefs this can occur in areas with higher salinity and correspondingly fewer macroscopic skeletal grains (Less and Buller 1972; Lees 1975). Salinity is also a controlling factor for bioturbation (Ekdale 1988). The fine lamination in facies E3 indicates there is little to no bioturbation (Droser and Bottjer 1993). Low bioturbation in shallow marine environments is reported where salinity is elevated or varies greatly because many animals that leave trace fossils are stenohaline (Ekdale 1988). The lack of bioturbation is likely responsible for the concentration of limonite and glauconite in laminations.

The color of the lime mudstone in facies E3 supports a shallow environment with shallowing upward cycles. The light gray lime mudstone does not contain any oxidized iron (apart from limonite on some laminae), but as the environment shallows the mottled and red lime mudstones have increasingly greater input of ferric iron; likely from wind-blown clay particles. The red lime mudstone indicates a shallow oxygenated environment (Turner 1980; Potter et al. 2005). The vertical color changes in facies E3 are gradational and indicate that these are Waltherian shallowing-upward cycles.

Facies E3 shares some similarities with a lagoon. It is muddy, laminated, laterally continuous parallel to the shoreline, and shallow; however, there is no evidence of extensive shoals or barrier islands that would have produced a true lagoon environment (Flügel 2010). The presence of facies E3 and restricted marine conditions may have been driven by restricted circulation across a nearly flat ramp, producing a salinity gradient (Lees and Buller 1972; Lees 1975; Flügel 2010).

Facies E3 gradationally overlies facies E1 indicating a landward transition from open marine to restricted marine conditions.

*Facies E4: unlaminated dolostone and microbialites*

**Description**—Facies E4 consists primarily of unlaminated dolostone, microbially laminated dolostone, and microbially laminated lime mudstone (Fig. 5d, e, f, 6). Unlaminated dolostone is light gray to pink and thin to thickly bedded. It is microcrystalline, giving it a porous texture. Unlaminated dolostone locally contains rip-up clasts composed of unlaminated dolostone.

Microbially laminated dolostone and lime mudstone display stromatolitic to thrombolitic textures (Fig. 6). Microbial structures may be large mounds up to ~0.5 m in diameter (Fig. 6a) or they may be relatively planar cryptalgal lamination. Microbially laminated dolostone and lime mudstone are thin to medium bedded and are frequently interbedded with unlaminated dolostone.

Facies E4 contains rare well-developed burrows of *Diplocraterion*, such as at Thermopolis (Fig. 5d). Sphaerolite cracks are locally found on the tops of lime mudstone beds (Fig. 5f). At Chimney Rock, thrombolitic lime mudstone contains tridactyl dinosaur footprints (Fig. 5e; Kvale et al. 2001).

Facies E4 ranges from 1–5 m thick. At Hyattville Alkali Road, Hyattville Road 49, and Cody, this facies is found in a collapse breccia, with gypsum between the brecciated fragments of facies E4. Facies E4 gradationally overlies facies E1 and E3, and it grades upwards into facies E5 and E7.

**Interpretation**—Facies E4 is interpreted to have been deposited on a tidal flat environment. The porous texture of the unlaminated dolostone is indicative of a peritidal setting (Carozzi 1989; Bachmann and Kuss 1998; Bachmann and Hirsch 2006; Flügel 2010). Microbial build-ups and laminations are also common in intertidal settings (Flügel 2010).

The sedimentary structures in facies E4 also provide strong evidence for an intertidal environment. Sphaeresis cracks form subaqueously from rapid changes in salinity, such as those found on tidal flats (Burst 1965; Plummer and Gostin 1981). The presence of tridactyl dinosaur footprints indicate that water depth was very shallow to periodically exposed (Kvale et al. 2001). In addition to footprints, *Diplocraterion* burrows have been found in Jurassic sediments in tidal flat deposits (Kvale et al. 2001; McMullen et al. 2014).

That facies E4 can gradationally overlie two other facies (E1 and E3) suggests two different interpretations. Where it overlies facies E1, it suggests that open marine environments passed directly landward into tidal flats. Where it overlies facies E3, it suggests that open marine environments passed landward into restricted shallow-subtidal environment and then into tidal flats. The difference between these two may reflect the dip of the ramp and the resulting degree to which circulation was limited.

### *Facies E5: red mudstone*

**Description**—Facies E5 contains red, maroon, brown, and green mudstone with beds of siltstone. Mudstone and siltstone are poorly laminated and unfossiliferous. Both weather to red mud and form slopes and valleys. Mudstone and siltstone locally contain gypsum nodules 2–50 cm in diameter. These nodules are locally partially or completely silicified (Fig. 7c). Gypsum stringers are also present. Facies E5 was analyzed by X-ray diffraction and contains dolomite, quartz, alkali feldspar, iron-rich clay minerals (vermiculite and illite), and hematite (Fig. 8). Dark gray hematite is visible on the fracture surfaces of many red and maroon mudstone fragments.

Where interbedded with facies E6, mudstone and siltstone beds are thin to massive. Where not interbedded, bedding is difficult to distinguish as a result of weathering.

Facies E5 may be less than 1 m to more than 10 m thick. Facies E5 gradationally overlies facies E4 and passes gradationally upwards into facies E7. Near the base of the Gypsum Spring Formation, facies E5 is interbedded with facies E6 (Fig. 7a, b).

**Interpretation**—Facies E5 is interpreted to have been deposited on supratidal flats, based on its composition and association. The ferric iron from clay minerals and hematite of facies E5 controls the red color, and it indicates there is a larger siliciclastic source and less carbonate influence for this facies compared to other facies. The oxidation of iron-rich clay minerals such as illite and vermiculite, as well as oxidation of finely disseminated hematite can produce a red pigmentation in supratidal deposits (Turner 1980; Blogett et al. 1993; Potter et al. 2005). The oxidation is likely contemporaneous with deposition or is a product of early diagenesis (Turner 1980; Blogett et al. 1993; Potter et al. 2005). The variation in mudstone coloration likely results from changes in redox conditions (Turner 1980; Potter et al. 2005). The green color indicates reduced iron, such as glauconite (Potter et al. 2005), although the presence

of glauconite could not be confirmed because it shares many characteristic X-ray peaks with illite.

Illite and vermiculite in the clay fraction of the mudstone can indicate an original source of weathering from felsic parent material (Hazen et al. 2013). Illite weathers from feldspars, and vermiculite weathers from muscovite and magnesium-rich micas (Hazen et al. 2013). Illite can alter to vermiculite in an alteration series that can end with vermiculite but often continues to smectite minerals (Robert 1973). This process is heavily influenced by oxidation and reduction (Robert 1973).

The land surface was infrequently wetted with marine waters as evidenced from the gypsum nodules and interbedding with facies E6 (Kendall and Harwood 1996; Kendall 2010). Facies E5 gradationally overlies facies E4, which indicates that tidal flats passed landward into supratidal flats.

#### *Facies E6: granular white gypsum*

**Description**—Facies E6 consist of thin to massively bedded, white, finely granular gypsum. There is no clear internal structure in most beds, but thicker beds may display a chickenwire texture that is enhanced by weathering. Gypsum beds are continuous over distances of 1–2 km, but more widely spaced columns do not contain the same number or thickness of gypsum beds. Gypsum beds range from 10 cm to 6 m in thickness, and the number of gypsum beds increases to the south. At Thermopolis, one gypsum bed passes laterally into facies E5 and E4. Gypsum beds usually form slopes, but can be cliff-forming (Fig. 8b). Facies E6 is interbedded with facies E5 near the base of the Gypsum Spring Formation (Fig. 8a, b), and the

number of gypsum beds decreases upwards. Where facies E6 overlies facies E1 and E4, the contacts are sharp.

Sr/Ca ratios show little variation among beds at Sheep Mountain South and Hyattville Alkali Road, but the ratio increases up-column at Trapper Creek (Fig. 9).

Similarly, principal components analysis of the elemental analyses of gypsum generally indicates little to no difference in composition among beds or localities (Fig 10). Two outlier samples had to be removed, as one (TrC-L-10.0) had anomalously high values of iron and aluminum, and another (TrC-L-21.5) had anomalously high values of zinc. The PCA shows no strong correlation among any of the elements in the analysis (Fig. 10a). The relatively compact shape of the data cloud indicates that the first and second principal components explain roughly similar amounts of variance (32% and 27%). When the sample scores from the first and second principal components are compared to stratigraphic position and latitude, variation within a bed overwhelms variation among beds or locations.

**Interpretation**—Facies E6 is interpreted to represent the episodic flooding of a supratidal area to create marine-fed coastal hypersaline ponds known as salinas. Strontium stable isotope analysis by Valentine (1997) indicated the evaporites in the Gypsum Spring Formation have a marine origin. The laterally discontinuity of gypsum beds indicates that facies E5 and E6 form a mosaic of supratidal flats and marine fed salinas (Kendall and Harwood 1996; Kendall 2010). The lack of macroscopic differences in the gypsum beds apart from the chickenwire texture, suggests a single environment of deposition for the gypsum. The chickenwire texture can be produced by nodular deposition or the alteration of gypsum to anhydrite and back to gypsum (Kendall 2010). Gypsum beds do not show any distinct lamination or other structure that would suggest primary deposition on a sabkha flat.

The Sr/Ca ratios for gypsum generally show high variance and no pattern up-column. The Sr/Ca ratios from Hyattville Alkali Road and Sheep Mountain South show large variation in the replicate samples from the same bed (Fig. 9a, b), suggesting that they deposited from a poorly-mixed shallow water brine in a salina or sabkha (Rosell et al. 1998). A well-mixed brine depositing gypsum subaqueously would be expected to have consistent Sr/Ca values within a bed (Rosell et al. 1998). Similarly, consistent values up-column would indicate repeated deposition from the same well-mixed brine source (Rosell et al. 1998). The Sr/Ca ratios for Hyattville Alkali Road and Sheep Mountain South are variable, ranging between 0.0010–0.0045, but there is no consistent pattern up-column, suggesting all beds were deposited in a poorly-mixed shallow water brine with the same original water source. The exception to this is Trapper Creek, where the Sr/Ca ratio increases upward. This could indicate the presence of two environments of deposition or changing seawater composition over time. However, replicate samples were not taken at Trapper Creek, and high variation in replicate samples would be unlikely to make a systematic pattern.

Similarly, principal components analysis of the cation to calcium ratios show that within-bed variation overwhelms variation up-column and variation among columns, with no strong patterns up-column or among columns. This supports the poorly-mixed shallow water brine deposition suggested by the Sr/Ca ratios. The consistently variable sample scores in the PCA suggest all beds up-column and among columns shared the same water source feeding the shallow-water brine environments.

An alternative explanation for the high variation within a bed and the absence of any trends in the gypsum composition is that the gypsum beds exposed at the surface have been weathering in the same environment. Gypsum is soluble at Earth-surface conditions (Kendall and

Harwood 1996; Kendall 2010), and this instability could result in alteration from weathering. Using core samples for elemental analysis may resolve this question.

The gradational vertical contacts of facies E6 with facies E5 and facies E4 indicates that marine-fed salinas were present across a land surface on tidal flats to supratidal flats. This is also supported by the lateral passage of facies E6 into facies E4 and E5, visible at Thermopolis.

#### *Facies E7: purple mudstone*

**Description**—Facies E7 contains very thin to thinly bedded purple mudstone (Fig. 7d, e, and f). The mudstone is structureless and beds are at most 20 cm thick. In excavated trenches, the mudstone displays fine mottling of light and dark purple. Clay-rich mudstone shows more defined mottling and a ped-like texture than does clay-poor mudstone (Fig. 7f). Facies E7 was analyzed by X-ray diffraction and contains iron-rich clay minerals, including illite and vermiculite, as well as hematite, dolomite, and quartz (Fig. 8). Facies E7 gradationally overlies facies E5 and E4 and the upper contact of facies E7 is always sharp.

**Interpretation**—Facies E7 is interpreted as a paleosol. Paleosols preserved in red bed deposits are commonly preserved with a purple color (Blodgett et al. 1993). The gradational base and sharp top of facies E7, as well as the ped-like structures in clay-rich mudstone support a paleosol interpretation (Retallack 1991; Potter et al. 2005). Although the lack of distinct structures in facies E7 makes it difficult to classify the paleosol (Nettleton et al. 2000), its association with reddened mudstones and gypsum deposits as well as the purple color suggest that it most likely formed in an arid environment as an aridisol (Turner 1980).

Facies E7 is mineralogically similar to the red and green mudstones of the supratidal flats, but is a distinctly different color. The purple coloration is common in paleosols and reflects

a larger hematite crystal size of ~ 10 microns in diameter (Torrent and Schwertmann 1987; Schwertmann 1993). The larger crystal sizes were presumably diagenetically produced (Torrent and Schwertmann 1987; Schwertmann 1993), given that there is no evidence of metamorphism. Diffuse distribution of hematite in mudstone is responsible for the color, suggesting the larger purple hematite crystals are diffuse in the mudstone there by giving the rock an overall purple coloring (Blogett et al. 1993; Schwertmann 1993). Illite can alter to vermiculite in soils, and this process is heavily influenced by oxidation and reduction (Robert 1973).

Facies E7 contains a single horizon of purple mudstone. Soil maturity is based on the number and differentiation of horizons within the soil, and this is usually thought to reflect development time (Jenny 1959). The purple mudstone containing only a single horizon can therefore be considered an immature soil that likely had a short development time.

## **DISCUSSION**

### *Facies model*

The facies model for the Middle Jurassic Gypsum Spring and Piper formations is the shallow-water portion of an evaporite-carbonate ramp with a gentle homoclinal dip (Fig. 11; Carozzi 1989, Bachmann and Kuss 1998; Bachmann and Hirsch 2006; Flügel, 2010). The most basinward facies is E1 interpreted as an open shallow-subtidal ramp, and its open-marine nature is indicated by the presence of abundant and diverse skeletal and non-skeletal carbonate grains (Lees and Buller 1972; Lees 1975; Carozzi 1989; Bachmann and Hirsch 2006; Flügel 2010).

Facies E1 passes laterally and landward into facies E3, interpreted as restricted shallow-subtidal ramp. The restricted shallow-subtidal facies lacks the diversity and abundance of grains seen in the open shallow subtidal facies. This is interpreted as resulting from increased salinity

(Less and Buller 1972; Lees 1975; Ekdale 1988). The salinity gradient is likely the result of the ramp morphology where slight changes in the dip of the ramp would have caused variations in circulation, creating locally elevated salinity (Read 1985).

Facies E2 is interpreted as forming near a fringing ooid shoal landward of the open and restricted shallow-subtidal facies (Fig. 11), although the setting of facies E2 is uncertain. It does not display the thickness or cross-bedding typical of an ooid shoal, and it occurs in so few columns that its facies relationships are unclear. Facies E2 may represent the distal portion of an ooid shoal that existed basinward of or laterally to the study area. The primary effect of this on the model would be to move the ooid zone to basinward of the open shallow-subtidal facies, making them the open and restricted shallow-subtidal part of a broad lagoon (Flügel 2010).

Facies E1, E2, and E3 pass landwards into facies E4, interpreted as tidal flats. Facies E4 passes landward into facies E5 and E6, interpreted as supratidal flats and marine-fed salinas respectively. In this innermost portion of the ramp, deposition consists primarily of terrigenous clay and silt, plus gypsum. The gypsum beds of facies E6 have a marine origin (Valentine 1997), but are discontinuous and encased in the mudstone of facies E5. This implies that supratidal flats surrounded the environment depositing gypsum. The gypsum also likely had only one depositional environment, owing to the morphological and geochemical uniformity of the gypsum deposits. These relationships suggest a coastal mosaic of supratidal flats and marine-fed salinas.

Facies E7 represents a paleosol with non-Waltherian relationships with all other facies. It is therefore interpreted to represent subaerial exposure of this ramp, with weathering of underlying facies, based on the mineralogical similarity to underlying facies. Facies E7 is sharply

overlain by E1, E3, E4 and E5, reflecting the position on the ramp when marine conditions resumed following transgression.

This evaporite-carbonate ramp differs somewhat from standard models (Flügel 2010). The additional restriction necessary to produce evaporite deposits in the inner ramp does not appear to come from ooid shoals or reef development (Read 1985; Carozzi 1989; Flügel 2010), but from restriction produced by an extremely shallow dip to the ramp. Slight local variations in the dip of the ramp could produce more isolated areas where the restricted shallow subtidal facies accumulated (Read 1985). A shallow dip would also produce the broad facies belts seen in the model and in the field (Fig. 11), as well as provide the additional restriction necessary for evaporite deposition.

This facies model differs from previous models for the Gypsum Spring and Piper formations in two ways. First, a single facies model is proposed here for the Gypsum Spring and the Piper Formations, compared to previous studies in which two or even three facies models were used (Doyle 1984; Parcell and Williams 2005). A single model simplifies the paleoenvironmental interpretation and is able to accommodate variation in deposits by local changes in ramp dip. It is also able to accommodate exposure and resumption of marine conditions without restructuring the facies model. Second, this model defines its facies association using a variation on a well-understood shallow carbonate system, the carbonate ramp. This allows an easy comparison of Jurassic paleoenvironments from Sundance Seaway to other carbonate ramp systems such as those in Europe during the Jurassic (Brigaud et al. 2009; Aghaei 2013; Brigaud et al. 2014).

### *Sequence stratigraphic interpretation*

The Middle Jurassic Gypsum Spring and Piper Formations contain three depositional sequences, the J-1, J-1a, and J-1b (Fig. 12, 13).

The regional combined J-0/J-1 sequence boundary separates the Triassic Chugwater Formation from the overlying Middle Jurassic Gypsum Spring Formation (Pipiringos and O'Sullivan 1978; Brenner and Peterson 1994; Kvale et al. 2001; Parcell and Williams 2005). The sequence boundary is recognized by a gentle angular unconformity, local relief of up to three meters, and the absence of the Early Jurassic Nugget Formation (J-0 sequence; Imlay 1952; Imlay 1956; Pipiringos and O'Sullivan 1978). The facies association changes across this boundary from coastal plain red beds to an evaporite-carbonate ramp (Lovelace and Lovelace 2012). At Trapper Creek and Chimney Rock, the boundary is well exposed and sharp, and it is immediately overlain by a 30 cm bed of reworked sandstone capped by gypsum. In most areas, this contact is covered and weathered, and the sequence boundary is placed at the base of the first gypsum bed or the top of the last red siltstone to sandstone bed, which marks the change in facies association.

The J-1 sequence contains the innermost ramp facies, facies E5 and E6, and the paleosol (E7). Above the J-1 sequence boundary is a thick (10–30 m) deposit of interbedded red mudstone to siltstone and gypsum beds (facies E5 and E6). Preservation of significant evaporite deposits requires a basal aquitard or a plume of constricted saline subsurface waters (Kendall, 2010). Transgression would cause marine incursion to move progressively landward to achieve a constricted plume (Kooi et al., 2000). The salinas and supratidal flat facies were therefore likely deposited during a marine transgression, making this the transgressive systems tract. Above the interbedded gypsum and mudstone beds is a thick (10–15 m) deposit of red mudstone locally

containing gypsum nodules. There are no identifiable flooding surfaces and the amount of gypsum decreases up-column, suggesting aggradational to possibly progradational stacking. This would make the red mudstone above the gypsum beds the highstand systems tract in the J-1 sequence. The maximum flooding surface is not identifiable in the J-1 sequence, but it likely occurs near the last gypsum bed where aggradational to progradational stacking patterns are suggested.

The J-1 sequence is capped by a purple mudstone (facies E7) in eight columns (Gypsum Spring Road North, Bighorn Canyon NRA, Spence Oilfield Road, County Road 1138, Sheep Mountain, Sheep Mountain South, Hyattville Alkali Road, and Hyattville Road 49). The purple mudstone is found at the same horizon in the columns, immediately below the first significant carbonate deposits. This suggests the paleosol developed simultaneously across an exposed surface rather than landward of the supratidal flats. This purple mudstone marks the subaerial exposure at the J-1a sequence boundary. Owing to the immaturity of the paleosol that reflects a short time of soil development (Jenny 1959), the duration of exposure on the J-1a sequence boundary was likely brief. In four other columns (Gypsum Spring Road, Little Sheep Mountain E, Chimney Rock, and Trapper Creek), the J-1a sequence boundary lacks a paleosol and is placed at a significant landward shift in facies, which places deeper-water facies unconformably over supratidal flat facies.

In the J-1a sequence immediately above the basal paleosol at Spence Oilfield Road and County Road 1138, there are one to two thin shallowing-upward parasequences of facies E4 and E5 overlain by a second paleosol. In these two columns, the sequence boundary is placed at the top of the first paleosol. The significant landward shift in facies was not observed in these columns until above the second paleosol. Owing to the position of these parasequences above the

sequence boundary and below the first significant flooding surface, they are interpreted as a possible preservation of the lowstand systems tract.

At all other points along the transect line, the J-1a sequence boundary coincides with the significant landward shift in facies. This shift is the first major flooding surface and is interpreted to represent the transgressive surface. In most measured sections, the base of the first carbonate facies or the top of the paleosol is a combined sequence boundary/transgressive surface.

Above the transgressive surface of sequence J-1a, there are multiple shallowing-upward parasequences of facies E1, E3, E4, and E5, which form a retrogradational stacking pattern. The most basinward parasequence in each section tends to deepen upwards. Retrogradationally stacked parasequences above a transgressive surface indicates these strata are part of the J-1a sequence transgressive systems tract. Retrogradational stacking is present until the base of the most basinward parasequence; above that, the parasequences are progradationally stacked. The change in stacking pattern from retrogradational to progradational indicates that the maximum flooding surface in J-1a lies at the base of the most basinward parasequence. This is marked by a lag of rip-up mud clasts at Gypsum Spring Road. In most other columns, the maximum flooding surface is marked by the greatest abundance of skeletal grains and peloids.

The strata above the J-1a maximum flooding surface consists of facies E1–E6 in progradationally stacked shallowing-upward parasequences. Progradational stacking above the maximum flooding surface indicates these strata are part of the J-1a sequence highstand systems tract.

The top of the J-1a highstand systems tract is capped with a chert horizon and a basinward shift in facies at the J-1b sequence boundary. The chert horizon capping the J-1a sequence highstand systems tract is present in eight columns (Bighorn Canyon NRA, Little

Sheep Mountain E, Spence Oilfield Road, Sheep Mountain South, Chimney Rock, Red Gulch, Hyattville Alkali Road, and Hyattville Road 49). The chert here has replaced anhydrite nodules and bedded gypsum, a common occurrence in arid to semi-arid climates that indicates subaerial exposure (Hesse 1990; El Khoriby 2005). The dissolution of gypsum and anhydrite by meteoric water at an exposed surface produces high pH pore waters that are able to dissolve silica. This silica-rich pore fluid will precipitate chert when it contacts acidic pore fluids (Knauth 1979; Hesse 1990; El Khoriby 2005). In an evaporitic setting, descending slightly acidic meteoric water is able to mix with silica-rich alkaline pore fluids drawn up to the near surface by high evaporation rates (Hesse 1990, Kendall 2010). The resulting deposit is known as a silcrete, which indicates prolonged exposure and flushing of meteoric waters (Hesse 1990). This replacement is not modern because no well-exposed lower gypsum beds are fully silicified, and the presence of bedded chert requires the original horizontality of the deposit.

In columns lacking this chert horizon, the J-1b sequence boundary is subtle. At Gypsum Spring Road North and Gypsum Spring Road, the two most basinward columns, the sequence boundary is marked by an abrupt basinward shift in facies that places supratidal flat and salina facies unconformably atop open shallow subtidal facies. At Trapper Creek, the J-1b sequence boundary is placed at the top of the last carbonate bed because the lack of identifiable flooding surfaces above this bed suggests a switch to aggradational stacking.

The J-1b sequence boundary is overlain by facies E5 of the Piper Formation. The lack of recognizable flooding surfaces in the sequence suggests an aggradational stacking pattern. Aggradational stacking above a sequence boundary could indicate that these deposits are part of the lower highstand systems tract or the upper lowstand systems tract. Based on the tendency for supratidal facies to occur in the highstand systems tract of the J-1 and J-1a sequences, the red

mudstone of the J-1b is likewise interpreted as the highstand systems tract. Silicified anhydrite nodules found in the Piper (in columns Little Sheep Mountain E and Sheep Mountain South) are likely produced by subsequent flushing of meteoric water in the supratidal flat environment of the Piper without prolonged exposure necessary to produce a silcrete. The top of the J-1b sequence lies at the sharp upper contact of the Piper Formation with the open-marine carbonates of the overlying Sundance Formation.

The contact between the Piper and Sundance formations was previously interpreted as the regional J-2 sequence boundary (Brenner and Peterson 1994; Parcell and Williams 2005; McMullen et al. 2014). The evidence for this sequence boundary includes truncation of the J-1b sequence boundary, an abrupt landward shift that places shallow-subtidal facies unconformably over supratidal flat facies, and a change in facies association from an evaporite-carbonate ramp to a carbonate ramp (McMullen et al. 2014). The J-2 sequence boundary is easily identified in the field by an abrupt color change from red to tan.

#### *Placement of the J-2 sequence boundary*

Uncertainty in the position of the J-2 sequence boundary has caused difficulty in correlation across Wyoming and into adjacent states (Pipiringos and O'Sullivan 1978; Brenner and Peterson 1994; Parcell and Williams 2005). When Pipiringos and O'Sullivan (1978) documented the major unconformities of the Jurassic of the western United States, they placed the J-2 unconformity between the Gypsum Spring Formation and the Piper Formation, or between the middle and upper unit (Piper Formation) of the Gypsum Spring Formation (Fig. 13). They noted that this boundary was marked by chert pebbles, and that it had low relief. This interpretation runs into difficulties in north-central Wyoming, where the Piper Formation pinches

out over the paleohigh of the Sheridan Arch (Brenner and Peterson 1994). Brenner and Peterson (1994) redefined the Mesozoic strata of the western United States in terms of marine cycles. In their interpretation, the Piper Formation should be grouped with the Gypsum Spring Formation in the first marine cycle, and the J-2 unconformity should be placed between the Piper Formation and the Sundance Formation (Brenner and Peterson 1994). This gave two possible positions for the J-2 unconformity. Kvale et al. (2001) recognized both positions as unconformities, but placed the J-2 at the lower surface, between the Gypsum Spring and Piper Formations.

Parcell and Williams (2005) took a sequence stratigraphic approach to the stratigraphy of the Gypsum Spring and Piper formations. They, supported by previous studies, identified a sequence boundary lower in the Gypsum Spring Formation, and they defined it as the J-1a sequence boundary (Doyle 1984). Parcell and Williams (2005) also placed the J-2 sequence boundary at the contact between the Piper Formation and the overlying Sundance Formation. Their interpretation did not address the presence of a third unconformity, the one separating the Gypsum Spring and Piper formations (Fig. 13).

In this study, all three of these surfaces are identified as sequence boundaries that record subaerial exposure and weathering. Additional evidence, the presence of a paleosol, is provided here for the J-1a sequence boundary identified by Parcell and Williams (2005). This study also confirms the reports of chert at the J-1b sequence boundary, originally the J-2 unconformity of Pipiringos and O'Sullivan (1978). The chert is not, however, in the form of pebbles, but represents replacement of evaporite minerals and development of a pedogenic surface at the newly named J-1b sequence boundary. This study also recognizes the sequence boundary between the Piper Formation and the overlying Sundance Formation, and identifies it as the regional J-2 sequence boundary, in agreement with recent work (Fig. 13; Parcell and Williams

2005; McMullen et al. 2001). This is the best placement of the J-2 because the contact between the Piper and Sundance Formations is more regionally traceable, it truncates the J-1b unconformity, and it marks a significant change in facies association across the boundary.

### *Evaporite deposits in a sequence stratigraphic framework*

This study provides a case study for the occurrence of a widespread ancient evaporite in a sequence stratigraphic framework. The gypsum deposits in the Gypsum Spring Formation are basin-marginal marine evaporite deposits that accumulated in salinas on the supratidal portion of an evaporite-carbonate ramp. The association with supratidal flat mudstone makes it clear that these evaporites are basin-marginal rather than basin-central (Kendall 2010). The placement of the gypsum beds in the transgressive systems tract in this study relies on the need for a plume of constricted saline subsurface waters, produced by the transgression, to preserve the gypsum as it was buried (Kooi et al. 2000; Kendall 2010). There are also small local gypsum beds in the highstand systems tract of sequence J-1a, but there is no evidence to assume a different environment of deposition for these gypsum beds.

The placement of evaporite deposits in the transgressive systems tract differs slightly from the idealized model from Handford and Loucks (1993), but is necessary to preserve multiple gypsum beds. The Handford and Loucks (1993) model of a carbonate-evaporite-siliciclastic arid ramp contains evaporites in the lowstand systems tract, the transgressive systems tract, and the highstand systems tract. The falling stage systems tract would be included within their highstand systems tract, as Handford and Loucks (1993) follow the system-tract nomenclature of Van Wagoner et al. (1990). In their idealized model, lowstand systems tract evaporite deposits are typically basin-central evaporites. The thick continuous deposits resulting

from deep basins and low water levels are not present in the Gypsum Spring Formation (Kendall 2010). In the Handford and Loucks (1993) model, the transgressive systems tract evaporite deposits are thin and isolated. While beds of gypsum in the Gypsum Spring Formation may be thin, the overall deposit of interbedded gypsum and mudstone is up to 30 m thick. Gypsum beds are laterally discontinuous, but not isolated from other gypsum beds. In the Handford and Loucks (1993) idealized model, the highstand systems tract evaporite deposits are similar to the Gypsum Spring, as they tend to make thicker and more continuous deposits, and one of the main environments of deposition is coastal salinas (Handford & Loucks 1993). The Handford and Loucks (1993) model, however, lacks a way to preserve the evaporites. Without a basal aquitard or a plume of saline subsurface waters, exposed and recently buried gypsum is vulnerable to dissolution from meteoric water or fresh groundwater (Kendall and Harwood 1996; Kendall 2010).

A more recent conceptual model from Catuneanu et al. (2011) predicts evaporite deposits in every systems tract. In their model of a mixed carbonate-evaporite basin, the evaporite deposits in the falling stage systems tract into the lowstand systems tract differ in their geometry and thickness from the evaporite deposits of the transgressive and highstand systems tracts. With slow drawdown in the basin, the falling stage and lowstand systems tracts contain a thick evaporite wedge adjacent to the shelf and a possible basin fill of thick continuous halite deposits. These thick and laterally extensive deposits are in contrast to the thinner less extensive subaqueous gypsum and sabkha deposits in the transgressive and highstand systems tracts. These deposits are depicted as more isolated and track landward and seaward with carbonate facies as the shoreline backsteps and subsequently progrades.

The gypsum deposits in the lower Gypsum Spring Formation are similar to the transgressive and highstand deposits of the Catuneanu et al. (2011) model, but contain some differences. The Catuneanu et al. (2011) model also lacks a method for preservation in the highstand systems tract, but it does not predict as thick or extensive of accumulations as the Handford and Loucks (1993) model. The Gypsum Spring gypsum deposits differ also in that they are a heterogeneous deposit of many smaller discontinuous gypsum beds rather than a homogeneous, but laterally restricted, unit predicted by the Catuneanu et al. (2011) model. The Handford and Loucks (1993) and Catuneanu et al. (2011) models are useful conceptually, but they demonstrate the difficulty of relying on too broad of a generalized model because actual systems will be variable and may require multiple local to regional facies models.

The difficulty in using a single idealized model to determine the sequence stratigraphic context of evaporite deposits is a common problem (Kendall 2010). The Permian Zechstein basin in north-central Europe and the North Sea is an example of these difficulties (Tucker 1991; Strohmenger et al. 1996). The evaporites in the Werra Series of the Zechstein basin formed on an evaporite-carbonate platform, where the gypsum and anhydrite deposits can be up to 300 m thick and laterally extensive (Strohmenger et al. 1996). Tucker (1991) interpreted these deposits as deposits from sabkhas, hypersaline lagoons, and salt lakes in the lowstand systems tract during complete drawdown. In contrast, Strohmenger et al. (1996) interpreted these evaporites as being deposited on a platform with shallow-water evaporites passing seaward into deep-water evaporites, with accumulation in the prograding highstand systems tract.

A key aspect in determining the sequence stratigraphic context of an evaporite deposit is knowing where it fits in the facies association. The facies that are associated with the evaporites should guide the bulk of the sequence stratigraphic interpretation and help place the evaporite

deposits in context. This may then require regional to local facies models to fully characterize evaporite deposits throughout an entire basin. This study is an example of using detailed facies analysis to the characterize evaporite deposits on an evaporite-carbonate ramp using both the facies association and the sequence stratigraphic context.

## CONCLUSIONS

1. The Aalenian–Bajocian Gypsum Spring and Piper formations represent an evaporite-carbonate ramp depositional setting. The facies model of this ramp includes open shallow-subtidal facies characterized by argillaceous lime mudstone, lime mudstone, skeletal wackestone, peloidal packstone, and skeletal packstone that passes depositionally updip into restricted shallow-subtidal facies. Restricted shallow-subtidal facies contain cycles of light gray to red laminated lime mudstone. Restricted shallow-subtidal facies pass landwards into intertidal flats with peritidal dolomite, syneresis cracks, *Diplocraterion* burrows, and dinosaur footprints. The tidal flats pass landward into a mosaic of supratidal flats and marine-fed salinas composed of red mudstone and gypsum.

2. The sequence stratigraphic interpretation resolves a regional correlation issue on the placement of the J-2 sequence boundary. The more regionally extensive J-2 boundary is placed at the contact between the Piper and Sundance formations, where there is a change in facies association and truncation of the J-1b sequence boundary. The J-1b sequence boundary is placed at the contact between the Gypsum Spring and Piper formations, and the J-1a is placed at the contact between the lower and middle units of the Gypsum Spring Formation. This study recognizes all three of the surfaces as sequence boundaries that record subaerial exposure and

weathering. It also provides additional evidence for the two sequence boundaries in the Gypsum Spring and Piper formations in the form of a paleosol at the J-1a surface and a pedogenic chert horizon at the J-1b surface.

3. This study provides a case study for the placement of a widespread evaporite deposit in a sequence stratigraphic framework. This interpretation places the gypsum beds of the lower Gypsum Spring in the transgressive systems tract of the J-1 sequence. This contrasts with idealized models, but accounts for a mechanism of preservation. In addition, it demonstrates the use of a detailed local facies interpretation and model of an evaporite-carbonate ramp to determine the sequence stratigraphic context of a widespread marine evaporite.

## CHAPTER 3

### CONCLUSION

The Aalenian–Bajocian Gypsum Spring and Piper formations were deposited on an evaporite-carbonate ramp. The facies model of this ramp includes open shallow-subtidal facies that pass positionally updip into restricted shallow-subtidal facies. Restricted shallow-subtidal facies pass landwards into intertidal flats, and then into a mosaic of supratidal flats and marine-fed salinas.

The sequence stratigraphic interpretation resolves a regional correlation issue on the placement of the J-2 sequence boundary. The more regionally extensive J-2 boundary is placed at the contact between the Piper and Sundance formations. The J-1b sequence boundary is placed at the contact between the Gypsum Spring and Piper Formations, and the J-1a is placed at the contact between the lower and middle units of the Gypsum Spring Formation. This study recognizes all three of the surfaces as sequence boundaries that record subaerial exposure and weathering, and it provides additional evidence for J-1a and J-1b sequence boundaries, a paleosol at the J-1a surface and a pedogenic chert horizon at the J-1b surface.

This study provides a case study for the placement of a widespread evaporite deposit in a sequence stratigraphic framework. This interpretation places the gypsum beds of the lower Gypsum Spring in the transgressive systems tract of the J-1 sequence. It demonstrates the use of a detailed local facies interpretation and model of an evaporite-carbonate ramp to determine the sequence stratigraphic context of a widespread marine evaporite.

## REFERENCES

- Aghaei A, Mahboubi A, Moussavi-Harami R, Heubeck C, Nadjafi M (2013) Facies analysis and sequence stratigraphy of an Upper Jurassic carbonate ramp in the Eastern Alborz range and Binalud Mountains, NE Iran. *Facies* 59:863–889
- Alsharhan AS, Kendall CGSC (1986) Precambrian to Jurassic rocks of Arabian Gulf and adjacent areas: their facies, depositional setting, and hydrocarbon habitat. *AAPG Bull* 70:977–1002
- Bachmann M, Hirsch F (2006) Lower Cretaceous carbonate platform of the eastern Levant (Galilee and the Golan Heights): stratigraphy and second-order sea-level change. *Cretaceous Res* 27:487–512
- Bachmann M, Kuss J (1998) The middle Cretaceous carbonate ramp of the northern Sinai: sequence stratigraphy and facies distribution. *Spec Publ – Geol Soc* 149:253–280
- Blakey RC (2014) Western interior seaway -- Jurassic and Cretaceous epicontinental seas of North America. <http://cpgeosystems.com/wispaleogeography.html>. Accessed 6 January 2015

Blogett RH, Crabaugh JP, McBride EF (1993) The color of red beds- a geologic perspective. In:  
Bigham JM, Ciolkosz EJ (eds) Soil color. SSSA Spec Publ 31:127–159

Brenner RL, Peterson JA (1994) Jurassic sedimentary history of the northern portion of the  
Western Interior Seaway, USA. In: Caputo MV, Peterson JA, Franczyk KJ (eds)  
Mesozoic systems of the Rocky Mountain region, USA. Rocky Mountain Section, Soc  
Sediment Geol, Denver, Colorado, pp 217–232

Brigaud B, Durllet C, Deconinck J-F, Vincent B, Pucéat E, Thierry J, Trouiller A (2009) Facies  
and climate/environmental changes recorded on a carbonate ramp: a sedimentological  
and geochemical approach on Middle Jurassic carbonates (Paris Basin, France). *Sediment  
Geol* 222:181–206

Burst JF (1965) Subaqueously formed shrinkage cracks in clay. *J Sediment Petrol* 35:348–353

Catuneanu O, Galloway WE, Kendall CGSC, Miall AD, Posamentier HW, Strasser A, Tucker  
ME (2011) Sequence stratigraphy: methodology and nomenclature. *Newsl Stratigr*  
44:173–245

Carozzi AV (1989) Carbonate rock depositional models: a microfacies approach. Prentice-Hall  
Inc., U.S.

- Doyle AB (1984) Stratigraphy and depositional environments of the Jurassic Gypsum Spring and Sundance Formations, Sheep Mountain Anticline area, Big Horn County, Wyoming. Thesis, University of Wisconsin-Milwaukee
- Droser ML, Bottjer DJ (1993) Trends and patterns of Phanerozoic ichnofabrics. *Annu Rev Earth Planet Sci* 21:205–225.
- Dunham RJ (1962) Classification of carbonate rocks according to depositional textures. In: Ham WE (ed) *Classification of carbonate rocks—a symposium*. AAPG Mem, pp 108–121
- Ekdale AA (1988) Pitfalls of paleobathymetric interpretations based on trace fossil assemblages. *Palaios* 3:464–472
- El Khoriby EM (2005) Origin of the gypsum-rich silica nodules, Moghra Formation, Northwest Qattara depression, Western Desert, Egypt. *Sediment Geol* 177:41–55
- Flügel E (2010) *Microfacies of carbonate rocks: analysis, interpretation and application*, 2nd edn. Springer, Germany
- Greene JF (1970) Stratigraphy and sedimentary tectonics of the Gypsum Spring Formation, Middle Jurassic, Fremont County, Wyoming. Thesis, University of Michigan-Ann Arbor

Guyer GS (1995) Paleoenvironments of the Jurassic Gypsum Spring Formation, Bighorn Basin, Wyoming. Thesis, Iowa State University of Science and Technology

Handford CR, Loucks RG (1993) Carbonate depositional sequences and systems tracts-responses of carbonate platforms to relative sea-level changes. In: Loucks RJ, Sarg JF (eds) Carbonate sequence stratigraphy: recent developments and applications: AAPG Mem 57:1–41

Hazen RM, Sverjensky DA, Azzolini D, Bish DL, Elmore SC, Hinnov L, Milliken RE (2013) Clay mineral evolution. *Am Mineral* 98:2007–2029

Hesse R (1990) Silica diagenesis: origin of inorganic and replacement cherts. In: McIlreath IA, Morrow DW (eds) Diagenesis. Geological Association of Canada, Ontario, pp 253–277

Imlay RW (1952) Correlation of the Jurassic formations of North America, exclusive of Canada. *Geol Soc Am Bull* 63:953–992.

Imlay RW (1956) Marine Jurassic exposed in Bighorn Basin, Pryor Mountains, and Northern Bighorn Mountains, Wyoming and Montana. *AAPG Bull* 40:562–599.z

Imlay RW (1980) Jurassic paleobiogeography of the conterminous United States in its continental setting. *U.S. Geol Surv Prof Pap* 1062:1–134

Jenny H (1959) *Factors of soil formation*. Dover Publications, Inc., New York

- Kendall AC, Harwood GM (1996) Marine evaporites: arid shorelines and basins. In: Reading HG (ed) *Sedimentary environments: processes, facies and stratigraphy*. Blackwell Science Ltd, London, pp 281–324
- Kendall AC (2010) Marine evaporites. In: James NP, Dalrymple RW (eds) *Facies models 4*. Geological Association of Canada, Canada, pp 541–576
- Knauth LP (1979) A model for the origin of chert in limestone. *Geology* 7:274–277
- Kooi H, Groen J, Leijnse A (2000) Modes of seawater intrusion during transgressions. *Water Resour Res* 36:3581–3589
- Kvale EP, Johnson AD, Mickelson DL, Keller K, Furer LC, Archer AW (2001) Middle Jurassic (Bajocian and Bathonian) dinosaur megatracksites, Bighorn Basin, Wyoming, USA. *Palaios* 16:233–254
- Lawton TF (1994) Tectonic setting of Mesozoic sedimentary basins, Rocky Mountain region, United States. In: Caputo MV, Peterson JA, Franczyk KJ (eds) *Mesozoic systems of the Rocky Mountain region, USA*, Rocky Mountain Section, Soc Sediment Geol, Denver, CO, pp 1–26
- Lees A, Buller AT (1972) Modern temperate-water and warm-water shelf carbonate sediments contrasted. *Mar Geol* 3:M67–M73

- Lees A (1975) Possible influence of salinity and temperature on modern shelf carbonate sedimentation. *Mar Geol* 19:159–198
- Lovelace DM, Lovelace SD (2012) Paleoenvironments and paleoecology of a lower Triassic invertebrate and vertebrate ichnoassemblage from the Red Peak Formation (Chugwater Group), central Wyoming. *Palaios* 27:636–657
- McMullen SK, Holland SM, O'Keefe FR (2014) The Occurrence of vertebrate and invertebrate fossils in a sequence stratigraphic context: the Jurassic Sundance Formation, Bighorn Basin, Wyoming, USA. *Palaios* 29:277–294
- Meyer JE (1984) The stratigraphy of the Gypsum Spring Formation (Middle Jurassic), northwestern Bighorn Basin, Wyoming. Thesis, University of Wyoming-Laramie
- Nelson CM (1963) Gypsum Spring and the "lower Sundance" formations, eastern Big Horn Mountains, Wyoming and Montana. Thesis, Michigan State University-East Lansing
- Nettleton WD, Olson CG, Wysocki DA (2000) Paleosol classification: problems and solutions. *Catena* 41:61–92
- Parcell WC, Williams MK (2005) Mixed sediment deposition in a retro-arc foreland basin: Lower Ellis Group (m. Jurassic), Wyoming and Montana, USA. *Sediment Geol* 177:175–194

Pedley M, Carannante G (2006) Cool-water carbonate ramps: a review. *Spec Publ – Geol Soc London* 255:1–9

Peters SE (2006) Macrostratigraphy of North America. *J Geol* 114:391–412

Pipiringos GN, O'Sullivan R (1978) Principal unconformities in Triassic and Jurassic rocks, western interior United States: a preliminary survey. U.S. Geol Surv Prof Pap 1035-A:A1–A29

Plummer P, Gostin V (1981) Shrinkage cracks: desiccation or syneresis? *J Sediment Res* 51:1147–1156

Potter PE, Maynard JB, Depetris PJ (2005) *Mud and Mudstones*. Springer-Verlag, Germany

Railsback BL (1993) A geologic numerical model for Paleozoic global evaporite deposition. *J Geol* 100:261–277

R Core Team (2013). *R: A language and environment for statistical computing*. R Foundation for Statistical Computing, Vienna, Austria. <http://www.R-project.org/>

Read JF (1985) Carbonate platform facies models. *AAPG Bull* 69:1–21

- Retallack G (1991) Untangling the effects of burial alteration and ancient soil formation. *Annu Rev of Earth and Planet Sci* 19:183–206
- Robert M (1973) The experimental transformation of mica toward smectite; relative importance of total charge and tetrahedral substitution. *Clays and Clay Miner* 21:167–174
- Rosell L, Orti F, Kasprzyk A, Playa E, Peryt TM (1998) Strontium geochemistry of Miocene primary gypsum; Messinian of southeastern Spain and Sicily and Badenian of Poland. *J Sediment Res* 68:63–79
- Schwertmann U (1993) Relations between iron oxides, soil color, and soil formation. In: Bigham JM, Ciolkosz EJ (eds) *Soil color*. SSSA Spec Publ 31:51–70
- Simone L (1980) Ooids: a review. *Earth-Sci Rev* 16:319–355
- Strohmenger C, Voigt E, Zimdars J (1996) Sequence stratigraphy and cyclic development of basal Zechstein carbonate-evaporite deposits with emphasis on Zechstein 2 off-platform carbonates (Upper Permian, Northeast Germany). *Sediment Geol* 102:33–54
- Tucker ME (1991) Sequence stratigraphy of carbonate-evaporite basins: models and applications to the Upper Permian (Zechstein) of northeast England and adjoining North Sea. *J Geol Soc (London, U.K.)* 148:1019–1036

Torrent J, Schwertmann U (1987) Influence of hematite on the color of red beds. *J Sediment Res* 57:682–686

Turner P (1980) Continental red beds. *Dev Sedimentol* 29:1–561

Valentine RB (1997) Chemostratigraphic trends of the Gypsum Spring Formation, Wyoming: implications for evaporite depositional and diagenetic environments. Thesis, University of Missouri-Columbia

Van Wagoner JC, Mitchum RM, Campion KM, Rahmanian VD (1990) Siliciclastic sequence stratigraphy in well logs, cores, and outcrops: concepts for high-resolution correlation of time and facies. *AAPG Spec Publ M7:III–55*

Warren JK (1989) *Evaporite sedimentology: importance in hydrocarbon accumulation*. Prentice-Hall Inc., New Jersey

Warren JK (2010) Evaporites through time: tectonic, climatic and eustatic controls in marine and nonmarine deposits. *Earth-Sci Rev* 98:217–2

Wilson JC (1955). *The Gypsum Spring Formation (Middle Jurassic) of western Wyoming*. Thesis, University of Kansas

**Fig. 1**—Paleogeographic reconstruction of western North America in the Bajocian Stage (~170 Ma), based on paleogeographic reconstructions of Blakey (2014). The boxed area shows the location of the study area (Fig. 2).



**Fig. 2**—Locations of Jurassic outcrop (blue) and measured sections in the Bighorn Basin of Wyoming. Cross-section A-A' in Fig. 12 is indicated. GSRN: Gypsum Spring Road North, GSR: Gypsum Spring Road, BNRA: Bighorn Canyon National Recreation Area, LSME: Little Sheep Mountain E, SOR: Spence Oilfield Road, 1138: County Road 1138, SM: Sheep Mountain, SMS: Sheep Mountain South, CR: Chimney Rock, TrC: Trapper Creek, RG: Red Gulch Dinosaur Tracksite, HAR: Hyattville Alkali Road, H49: Hyattville Road 49. See Appendix A for locality coordinates.

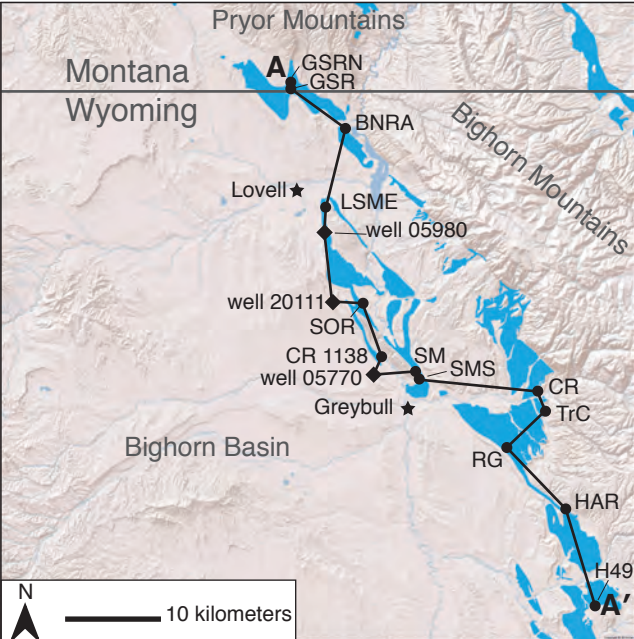


**Fig. 3**— Outcrop and thin section photographs of facies E1. All scale bars in thin section images are 1 mm. **a** Outcrop photograph of deepening and thickening upward lime mudstone to peloidal packstone and skeletal wackestone at Gypsum Spring Road North. **b** Argillaceous lime mudstone deepening upward (right) to peloidal packstone and skeletal wackestone at Gypsum Spring Road. **c** Finely laminated lime mudstone in plane polar light and quarter wavelength retardation plate. Chimney Rock. **d** Skeletal wackestone with ostracods in cross-polar light and quarter wavelength retardation plate. Gypsum Spring Road. **e** Clotted peloidal packstone in cross-polar light, County Road 1138. **f** Skeletal packstone in plane polar light and quarter wavelength retardation plate. E: echinoderm plates. Q: quartz silt. All other skeletal grains are bivalves.

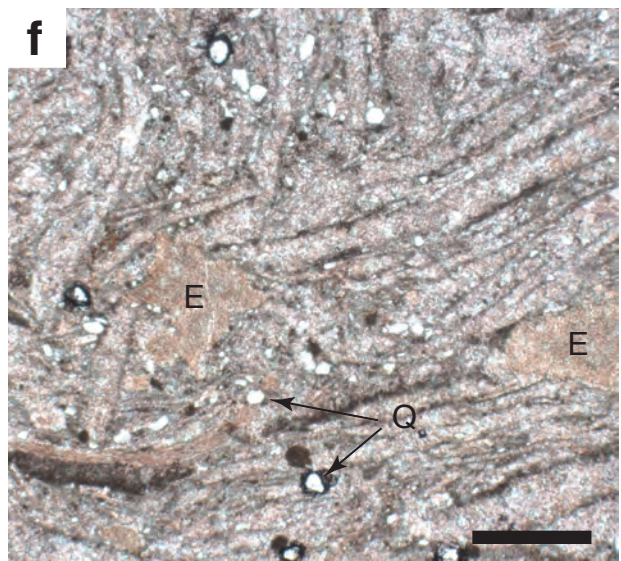
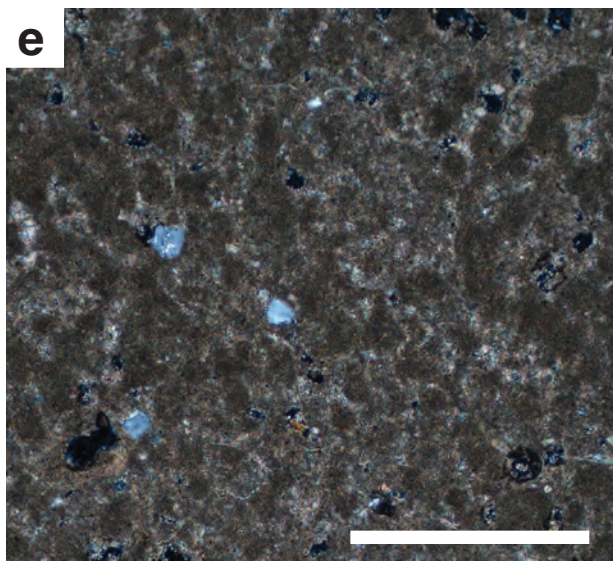
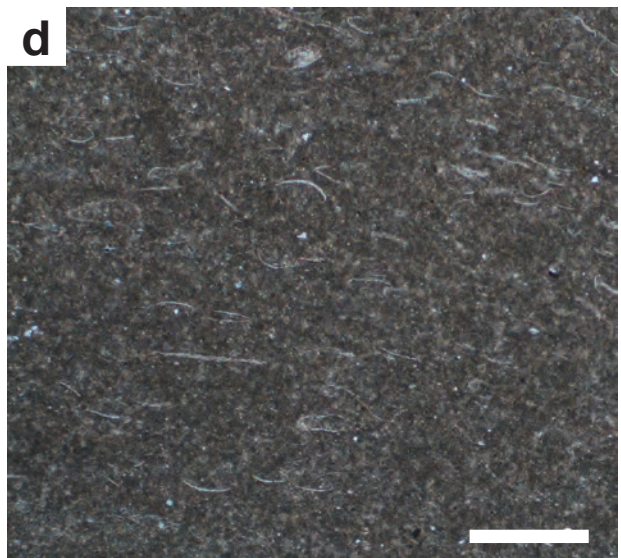
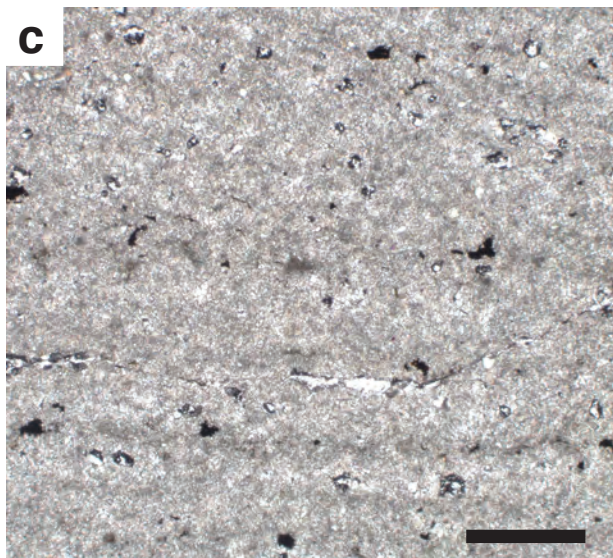
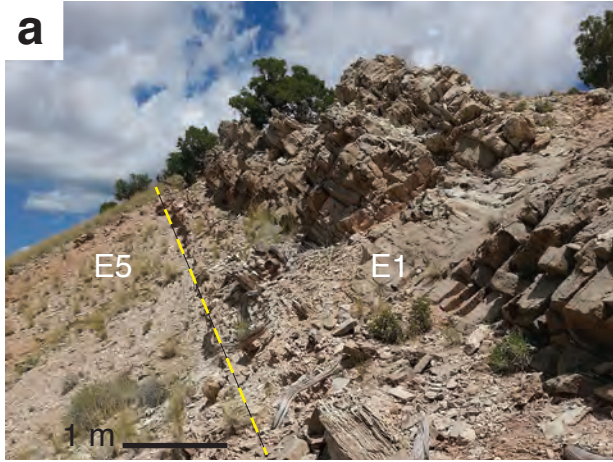


**Fig. 4**— Outcrop and thin section photographs for facies E2. All scale bars in thin section images are 1 mm. **a** Outcrop photograph of a resistant ooid grainstone bed forming a hogback at Sheep Mountain South. **b** Outcrop photograph of the limited lateral extent of facies E2 at Gypsum Spring Road North. **c** Ooid grainstone in cross-polar light, with concentric (c) ooids with micritic layers and radial (r) ooids with crystalline layers. H: unidentified ooid core depicting a regular hexagonal cross-section, Gypsum Spring Road-L-38.5s. **d** Ooid grainstone in cross-polar light. Yellow arrow indicates several overlapping ooids that have merging grain boundaries produced by pressure solution. Concentric (c) ooids and radial (r) ooids are shown as well along with coated skeletal grains (s). Gypsum Spring Road-L-38.5s. **e** Ooid grainstone in cross-polar light. The cement in the ooid grainstone at Sheep Mountain South-L-40.0 is primarily calcite (Cal), but there is also gypsum (G) filling void space where calcite cement has been dissolved. A: recrystallized partially rehydrated anhydrite grain with calcite and anhydrite inclusions. Ooid cores include quartz silt (Q) and chert (Ch). Oo: broken radial ooid. **f** Ooid grainstone (found in float) in plane-polar light. This grainstone is finer grained and contains more peloids and uncoated skeletal grains than ooid grainstone from Gypsum Spring Road and Sheep Mountain South, and Trapper Creek-L-5.0.

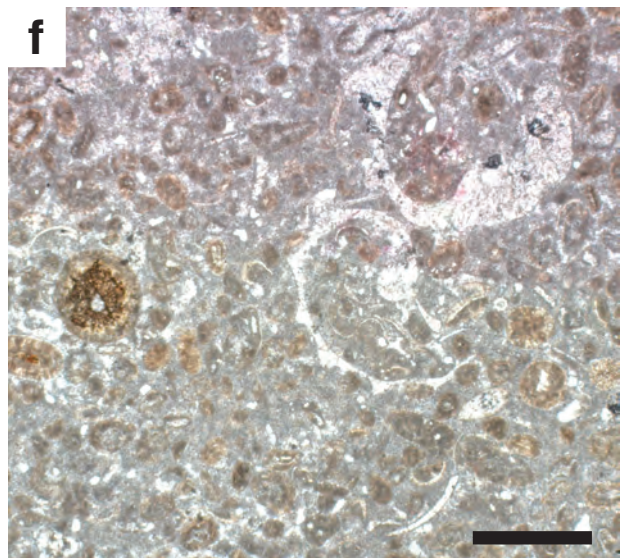
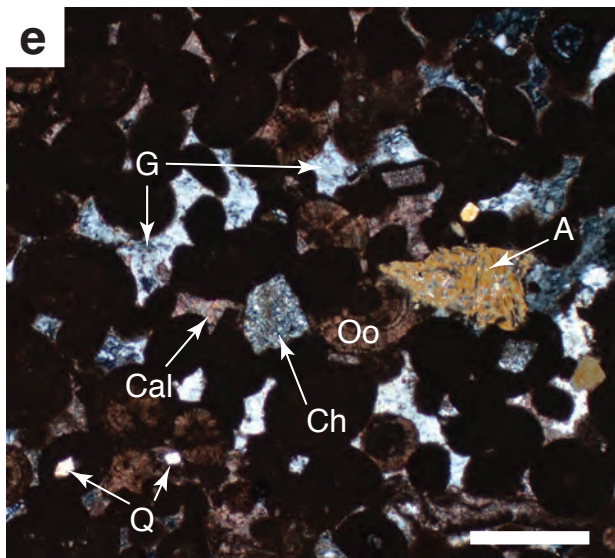
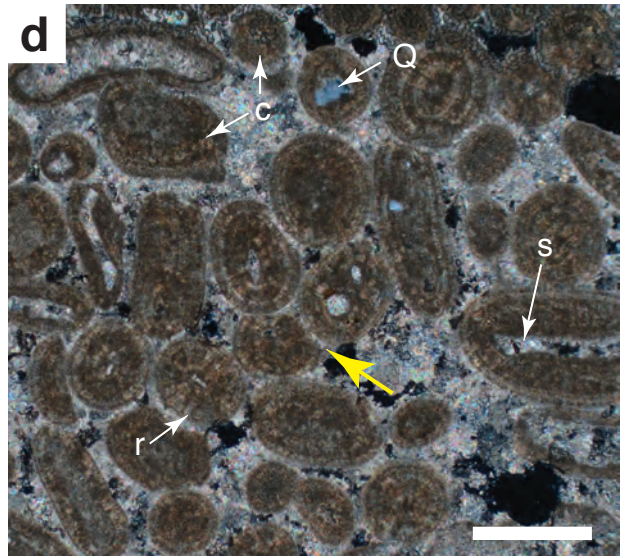
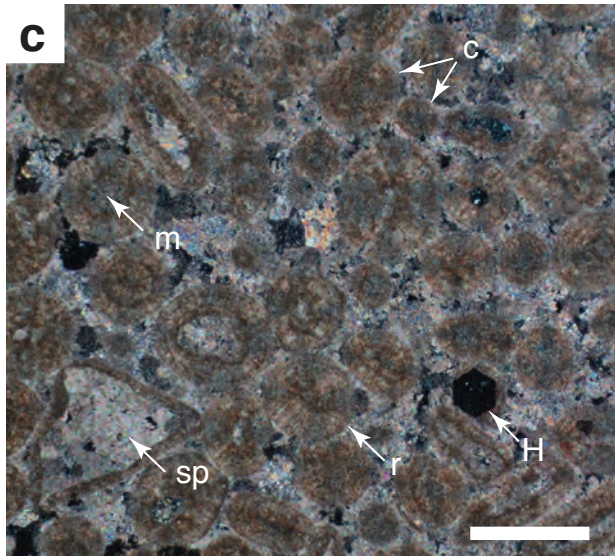
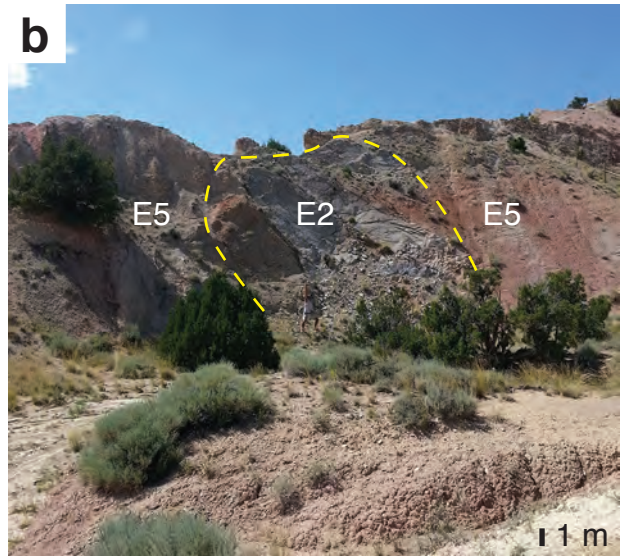


**Fig. 5**— Outcrop and structure photographs for facies E3 and E4. **a** Outcrop photograph of facies E3 light gray lime mudstone grading into mottled then red lime mudstone at Bighorn Canyon National Recreation Area. The top grades into facies E4 and the bottom has a sharp contact with facies E5. **b** Outcrop photograph showing thin laminae and very thin beds and at Gypsum Spring Road. **c** Light gray lime mudstone with abundant small moldic bivalves (mostly *Pleuromya*) and limonite stain. **d** Facies E4 with yellow arrows pointing to tops of *Diplocraterion* burrows at Thermopolis supplementary section. **e** Facies E4 with a tridactyl dinosaur footprint, from the Gypsum Spring Formation tracksite near Red Gulch (Kvale et al. 2001). **f** Facies E4 with synaeresis cracks on a lime mudstone from Sheep Mountain.

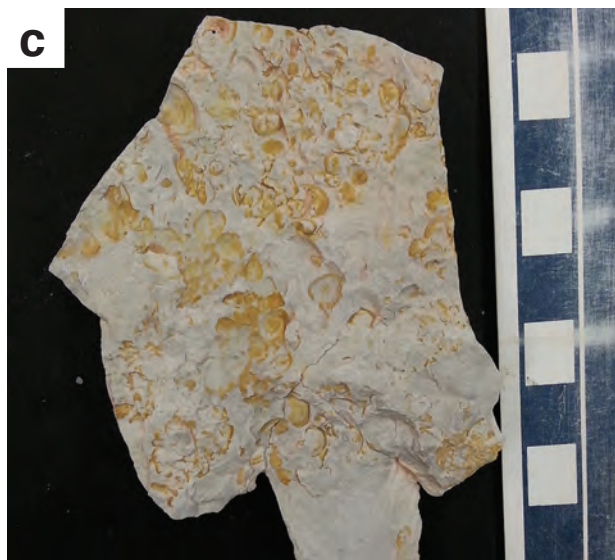
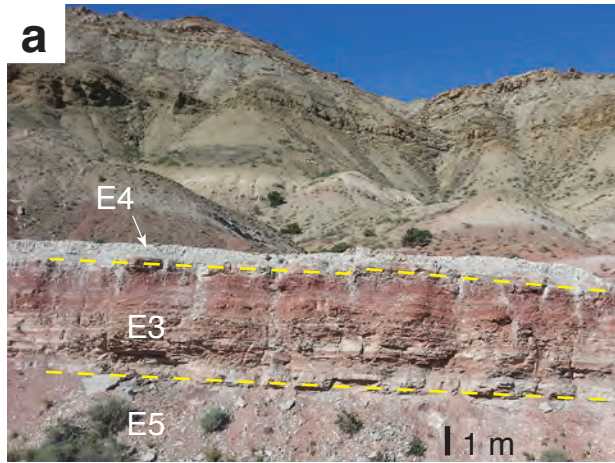


**Fig. 6**—Outcrop and thin section photographs for facies E4, continued. All scale bars in thin section images are 1 mm. **a** Mounded stromatolitic dolostone at Chimney Rock. Mounds are approximately 0.5 m in diameter. **b** Macroscopic clotted thrombolitic texture in dolostone at Chimney Rock. **c** Facies E4 with fine microbial laminations in lime mudstone (plane-polar light, quarter wavelength retardation plate) from County Road 1138-L-f23. **d, e** Facies E4 with clotted but laminated microbial texture from Trapper Creek samples 42.4 and 40.8 respectively. D is under plane polar light and quarter wavelength retardation plate. E is under cross-polar light and quarter wavelength retardation plate. **f** Facies E4 showing clotted but laminated lime mudstone with gypsum (blacks and grays) deposited in void space from Trapper Creek-L-40.8. (cross-polar light).

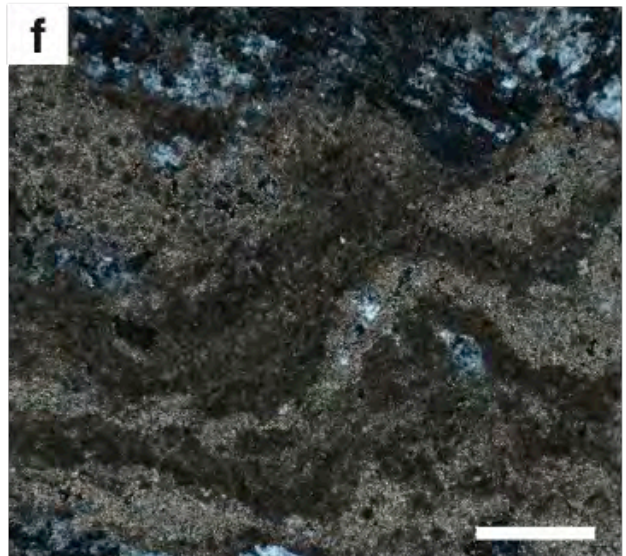
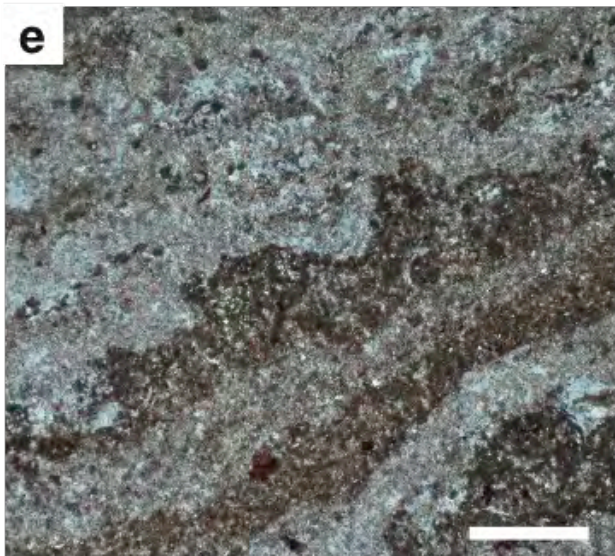
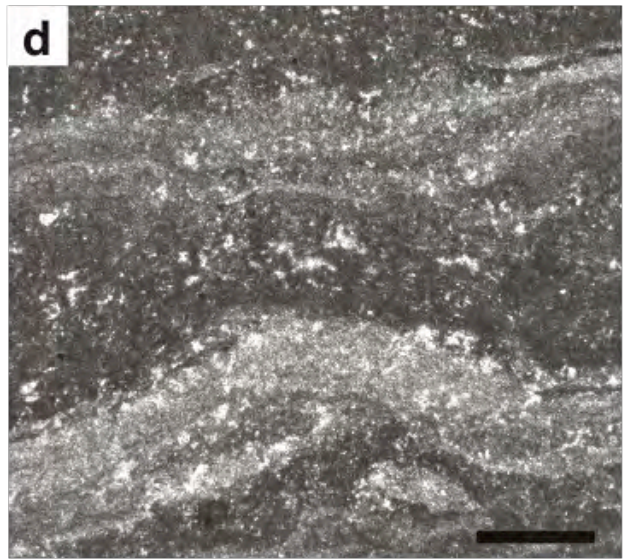
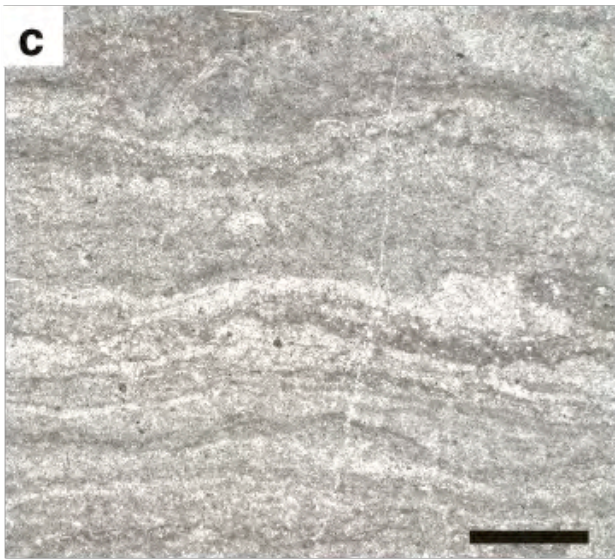
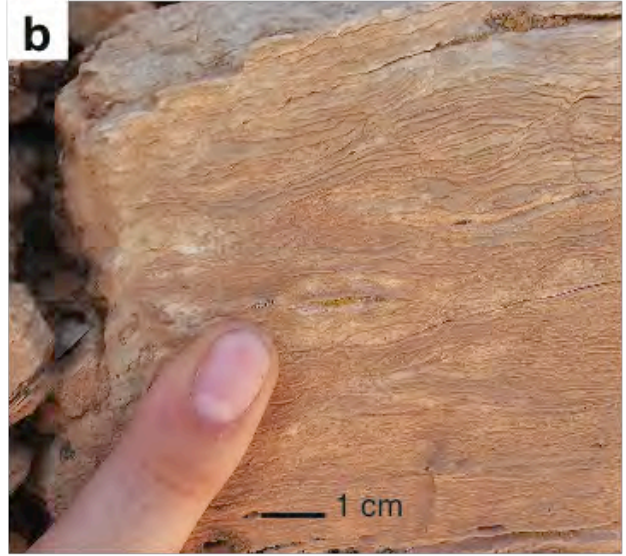


**Fig. 7**—Outcrop and feature photographs for facies E5, E6, and E7. **a** Interbedded gypsum (E6) and mudstone (E5) at County Road 1138. Gypsum beds form cliffs at this location. **b** Interbedded mudstone and gypsum at Bighorn Canyon NRA; here gypsum beds form slopes and are delineated by vegetation growing in the mudstone interbeds. **c** Silicified gypsum or anhydrite nodule from Hyattville County Road 49. **d** Facies E7, purple mudstone with a gradational base and sharp top, from Sheep Mountain South. **e** Facies E7, a purple mudstone with a gradational base and sharp top, from County Road 1138. **f** A fragment of facies E7 with a high clay content that shows a ped-like weathering pattern from sample SM-L-4.5 at Sheep Mountain.

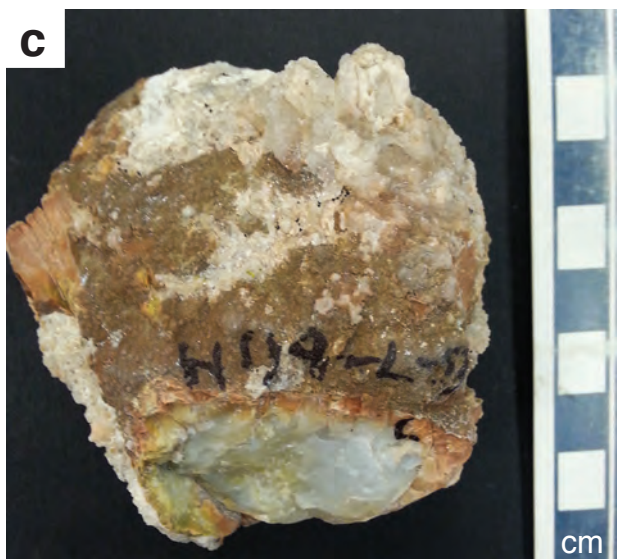
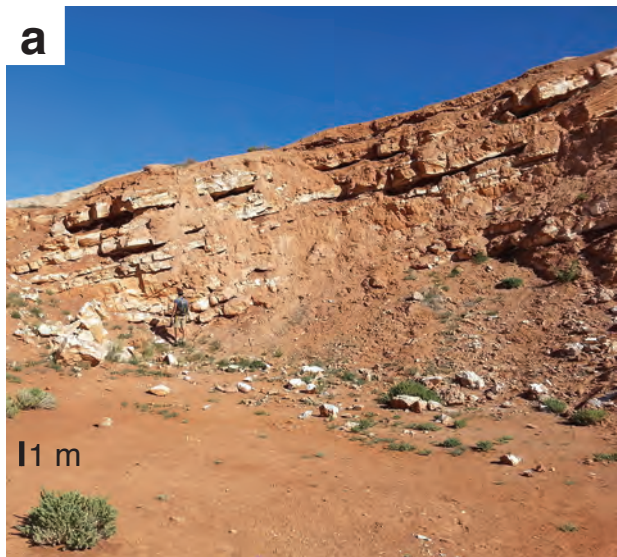


**Fig. 8**—X-ray diffraction of representative mudstones of the Gypsum Spring and Piper Formations. Two samples of each of purple mudstone (**a**), red mudstone (**b**), and green mudstone (**c**) were analyzed. Mineralogy of characteristic peaks are indicated. GSRN-L-38.3 bulk: Gypsum Spring Road North from meter 38.3. SM-L-4.5: Sheep Mountain from meter 4.5. GSR-L-9.1: Gypsum Spring Road from meter 9.1. LSME-L-28.5: Little Sheep Mountain E from meter 28.5. RG-L-6.4: Red Gulch from meter 6.4. TrC-L-40.0: Trapper Creek from meter 40.0. Curves have been kAlpha2 stripped and corrected for displacement using a zincite internal standard.

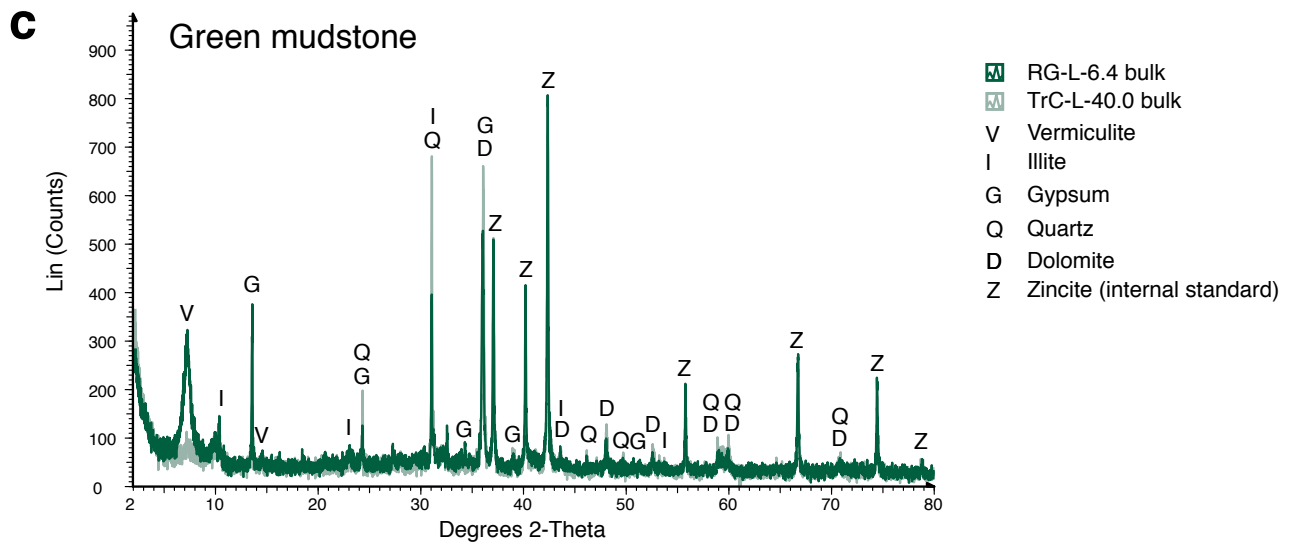
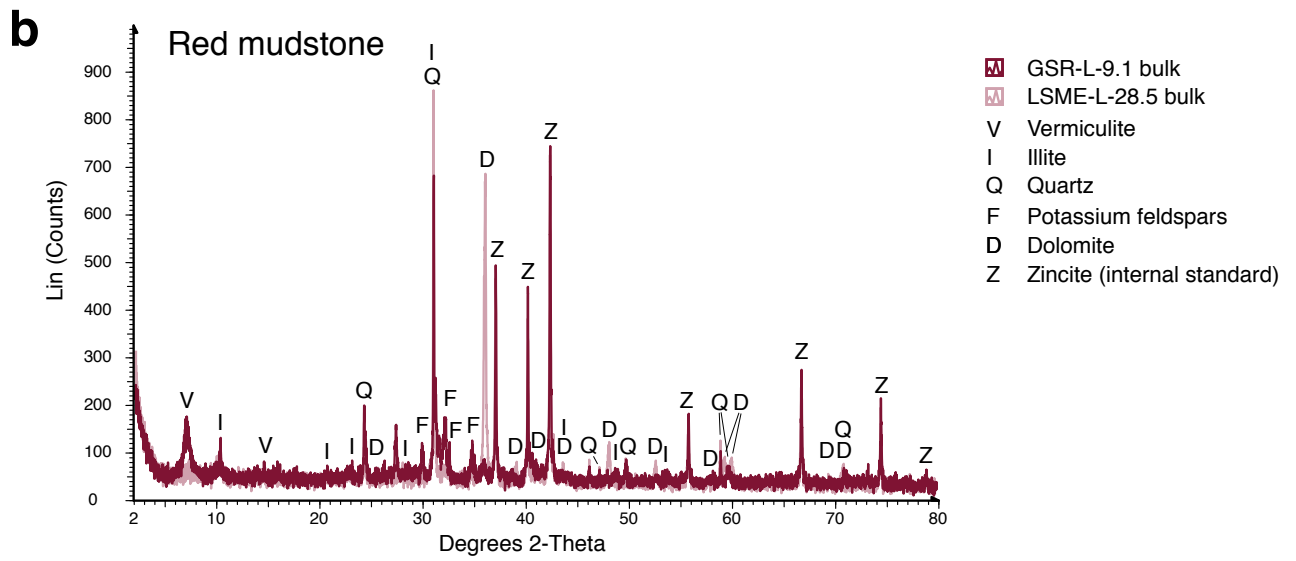
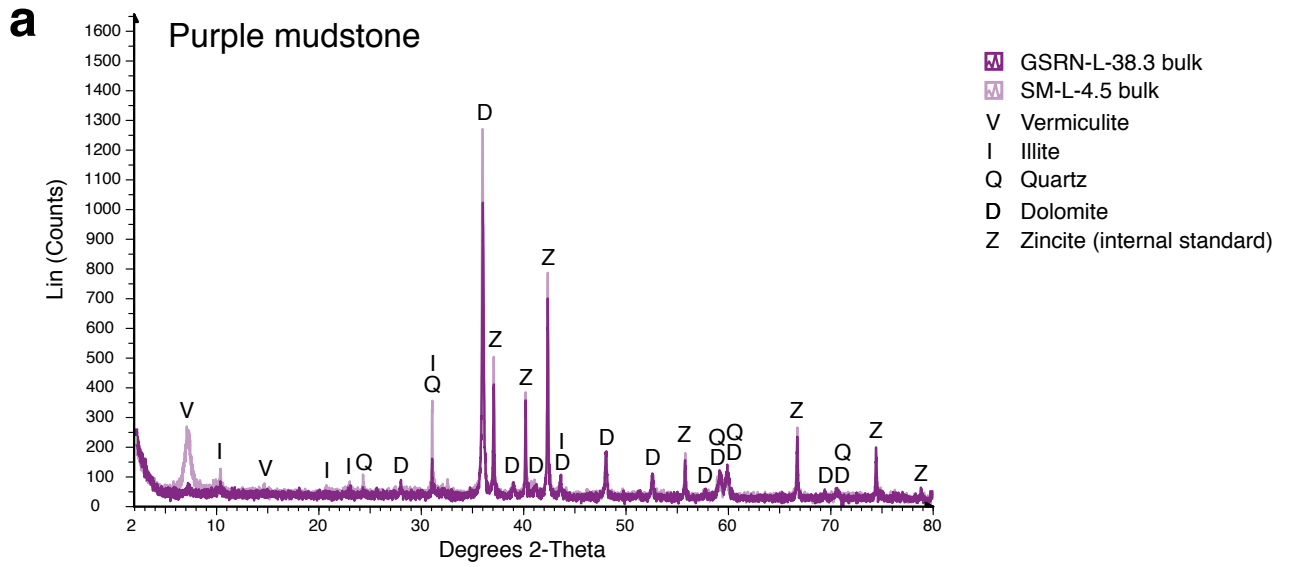


**Fig. 9**—Strontium to calcium ratios for columns where more than three gypsum beds were sampled. **a** Sr/Ca vs. stratigraphic position at Trapper Creek. **b** Sr/Ca vs. stratigraphic position at Sheep Mountain South. **c** Sr/Ca vs. stratigraphic position for the Hyattville Alkali Road column. See Appendix B for all sample cation concentrations.

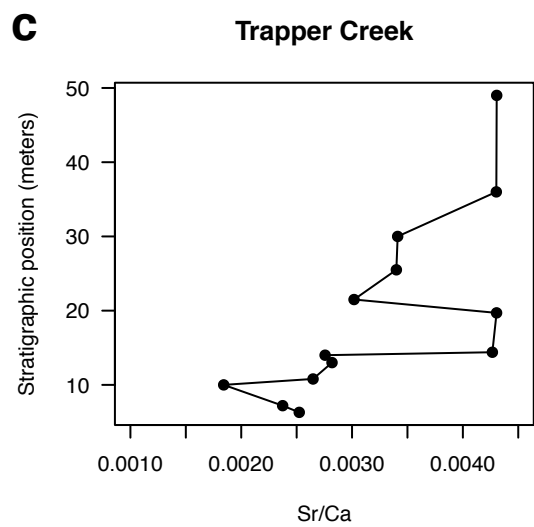
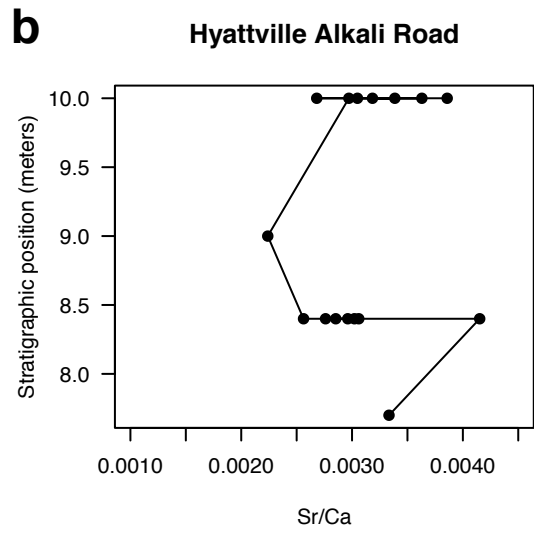
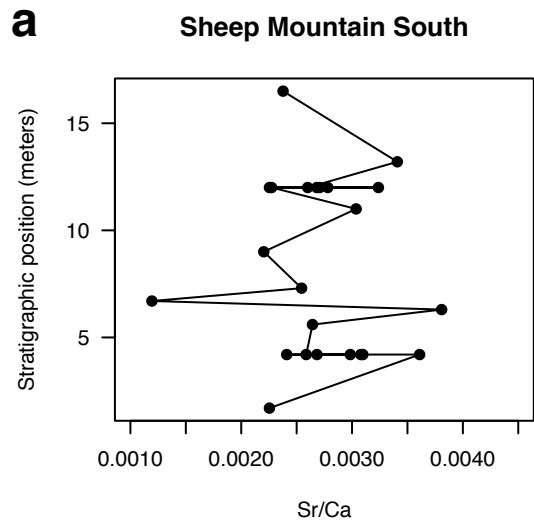


**Fig. 10**—Principal components analysis of cation to calcium ratios from the lower gypsum beds of the Gypsum Spring Formation. All data points are sample scores. **a** PCA1 vs. PCA2. Sample scores shown as blue dots, with variable loadings shown as red arrows. **b** PCA1 vs. PCA2 with samples colored by replicates and the centroid of each replicate set plotted. **c** PCA1 vs. stratigraphic position with samples colored by replicates. **d**) PCA2 vs. stratigraphic position with samples colored by replicates. **e** PCA1 vs. Latitude with samples colored by replicates. See Appendix A for coordinates of column locations. **f** PCA2 vs. latitude with samples colored by replicates. See Appendix A for coordinates of column locations. See Appendix B for all sample cation concentrations.

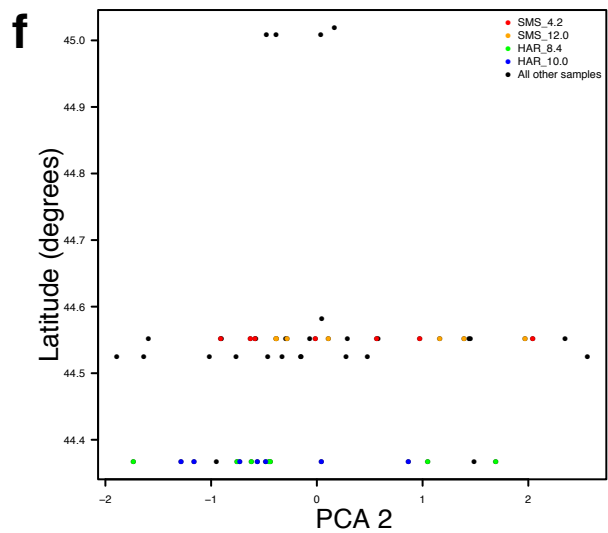
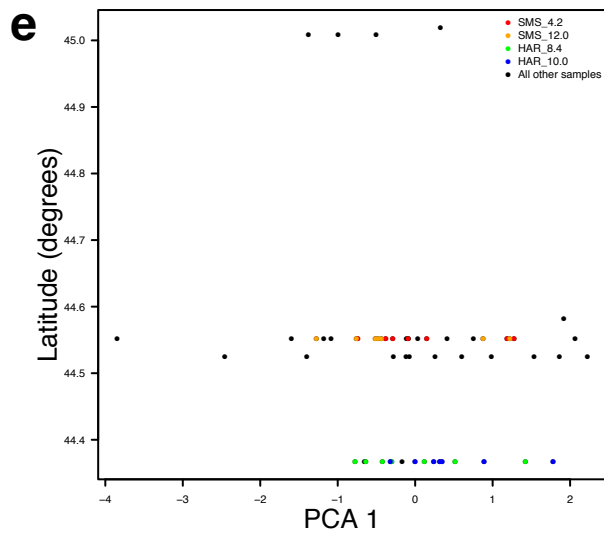
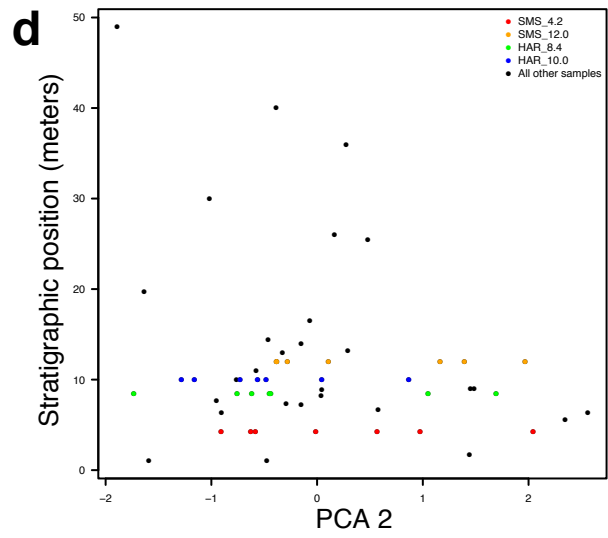
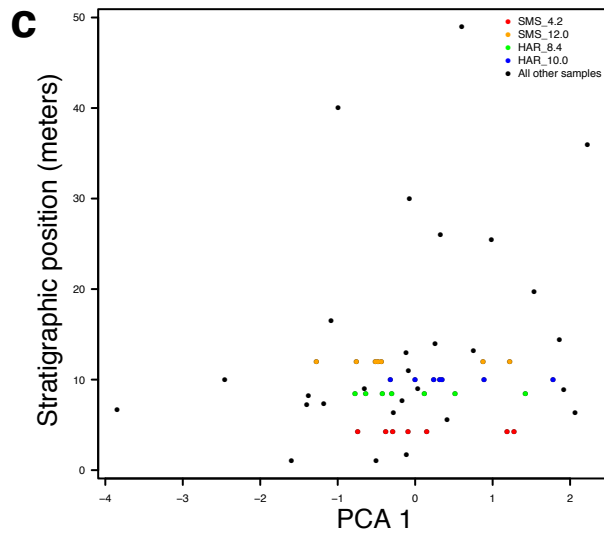
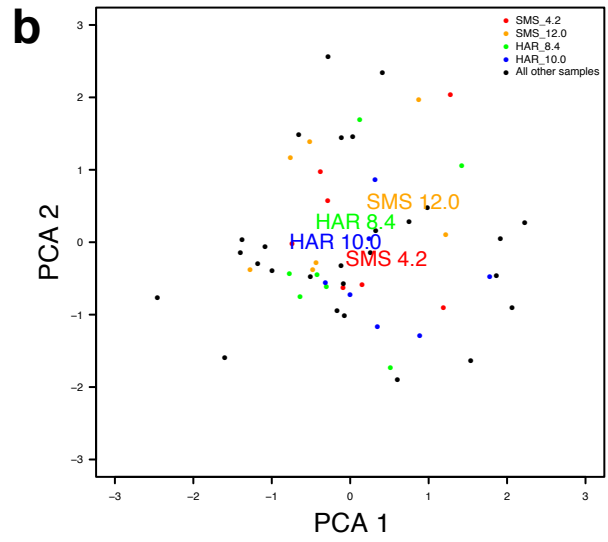
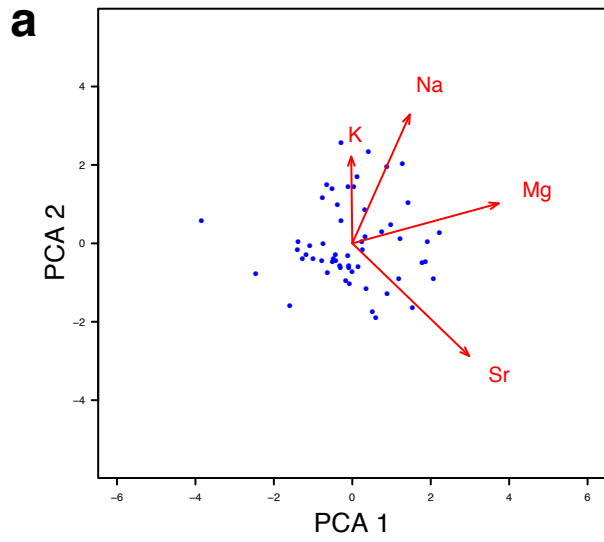


**Fig. 11**—Facies model showing interpreted lateral relationships among facies in the Gypsum Spring and Piper formations. Facies depicted in association on an evaporite-carbonate ramp.

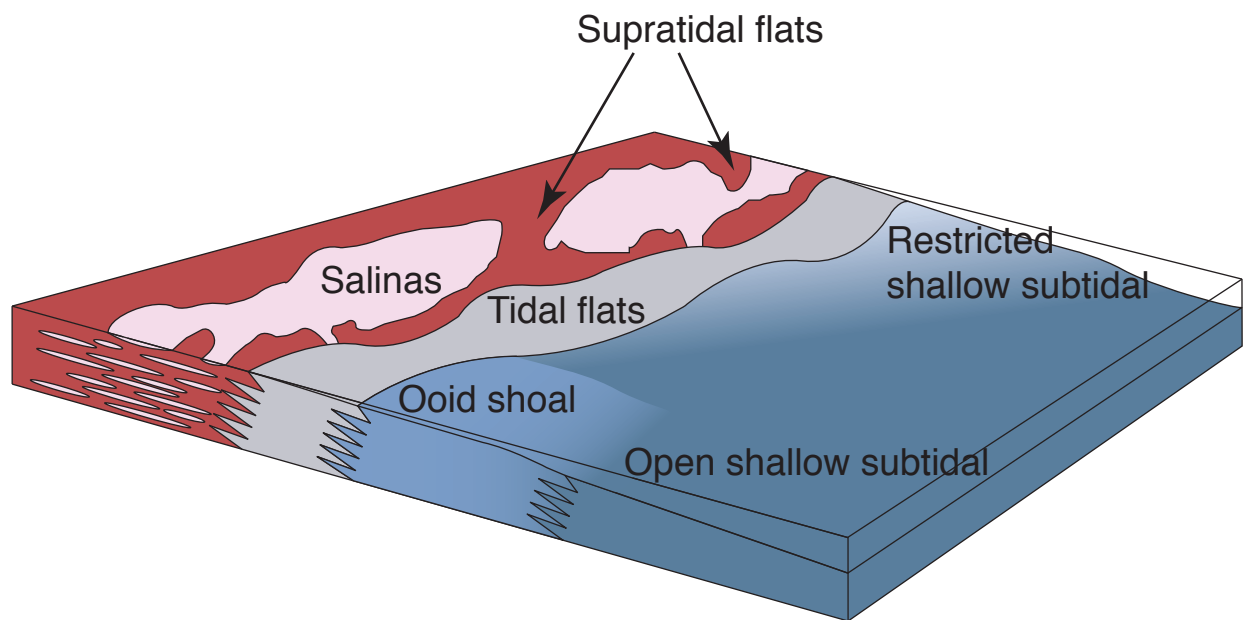
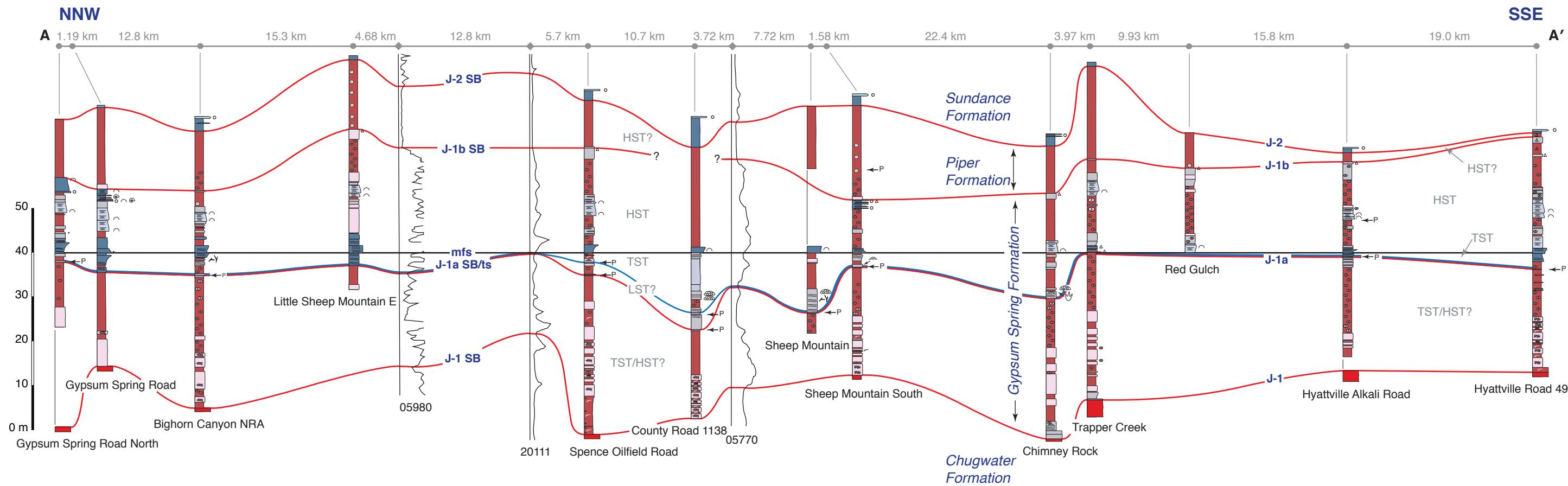


**Fig. 12**—Stratigraphic cross-section and sequence stratigraphic interpretation of the Gypsum Spring and Piper formations on the eastern margin of the Bighorn Basin. SB: sequence boundary. ts: transgressive surface. mfs: maximum flooding surface. LST: lowstand systems tract. TST: transgressive systems tract. HST: highstand systems tract.



**Evaporite Carbonate Ramp  
Facies Association**

- E7: Paleosol
- E6: Marine fed salinas
- E5: Supratidal flats
- E4: Tidal flats
- E3: Restricted shallow subtidal
- E2: Ooid zone
- E1: Shallow subtidal

**Structures and Fossils**

- Gastropod
- Bivalve
- Gypsum stringers
- Chickenwire gypsum
- Gypsum nodules
- Silicified anhydrite nodules
- Lithoclast
- Ooid
- Chert
- Syneresis cracks
- Paleosol
- Planar lamination
- Wavy lamination
- Thrombolitic microbial lamination
- Stromatolitic microbial lamination
- Trackway

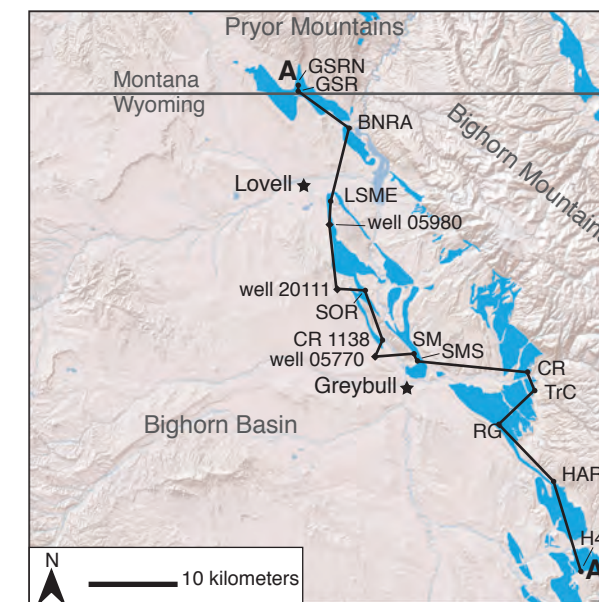


**Fig. 13**—Revised chronostratigraphic chart for the Middle Jurassic of eastern Wyoming, with time scale based on the 2014 international chronostratigraphic chart by the International Commission on Stratigraphy. Chronostratigraphy of units is based on Pipiringos and O’Sullivan (1978), Imlay (1952), Imlay (1980), Brenner and Peterson (1994), Kvale et al. (2001), and Parcell and Williams (2005).



APPENDIX A  
COLUMN LOCATIONS

<b>Locality</b>	<b>Longitude</b>	<b>Latitude</b>
Gypsum Spring Road North	-108.424	45.019
Gypsum Spring Road	-108.424	45.009
Bighorn Canyon NRA	-108.280	44.955
Little Sheep Mountain E	-108.304	44.819
Spence Oilfield Road	-108.188	44.667
County Road 1138	-108.127	44.581
Sheep Mountain	-108.043	44.564
Sheep Mountain South	-108.033	44.552
Chimney Rock	-107.751	44.557
Trapper Creek	-107.728	44.525
Red Gulch	-107.807	44.457
Hyattville Alkali Road	-107.652	44.367
Hyattville 49	-107.555	44.211
Cody	-109.057	44.454
Thermopolis	-108.191	43.672

## APPENDIX B

### ELEMENTAL ANALYSIS RAW DATA

All elemental values in ppm

<b>Sample</b>	<b>strat.position</b>	<b>latitude</b>	<b>Al</b>	<b>B</b>	<b>Ba</b>	<b>Ca</b>
DI_blank			0.002	1.485	0	0.001
GSRN_L_26.0	26	45.0195	-0.007	1.341	0.002	97.794
GSR_L_1.1	1.1	45.0087	-0.005	1.282	0.002	112.763
GSR_L_8.2	8.2	45.0087	-0.008	1.216	0.002	132.871
GSR_L_40.0	40	45.0087	-0.006	1.583	0.003	156.012
1138_L_8.9	8.9	44.5813	-0.007	1.271	0.004	140.588
TrC_L_6.3	6.3	44.5254	-0.008	1.794	0.002	142.262
TrC_L_7.2	7.2	44.5254	-0.008	1.015	0.002	137.325
TrC_L_10.0	10	44.5254	0.093	1.166	0.002	191.127
TrC_L_10.8	10.8	44.5254	-0.005	1.079	0.003	111.4
TrC_L_13.0	13	44.5254	-0.007	1.305	0.002	136.205
TrC_L_14.0	14	44.5254	-0.007	1.479	0.002	124.045
TrC_L_17.4	14.4	44.5254	-0.006	1.952	0.006	154.231
TrC_L_19.7	19.7	44.5254	-0.01	0.783	0.006	177.959
TrC_L_21.5	21.5	44.5254	-0.006	1.923	0.004	126.896
TrC_L_25.5	25.5	44.5254	-0.003	1.998	0.003	150.591
TrC_L_30.0	30	44.5254	-0.007	1.363	0.005	129.554
TrC_L_36.0	36	44.5254	-0.005	2.046	0.011	138.306
TrC_L_49.0	49	44.5254	-0.007	1.498	0.011	137.963
SM_L_1.0	1	44.5512	-0.005	1.272	0.002	110.279
SMS_L_1.7	1.7	44.5512	-0.006	2.038	0.002	162.332
SMS_L_4.2A	4.2	44.5512	-0.005	1.659	0.002	100.832
SMS_L_4.2B	4.2	44.5512	-0.007	1.384	0.005	140.618
SMS_L_4.2C	4.2	44.5512	-0.006	1.325	0.002	104.556
SMS_L_4.2	4.2	44.5512	-0.006	1.88	0.004	173.661
SMS_L_4.2D	4.2	44.5512	-0.007	1.626	0.004	146.256
SMS_L_4.2E	4.2	44.5512	-0.008	1.711	0.004	160.837
SMS_L_4.2F	4.2	44.5512	-0.002	1.887	0.002	93.961
SMS_L_5.6	5.6	44.5512	-0.008	1.652	0.002	113.496
SMS_L_6.3	6.3	44.5512	-0.006	1.2	0.003	122.357
SMS_L_6.7	6.7	44.5512	-0.004	1.022	0.001	91.289

<b>Sample</b>	<b>strat.position</b>	<b>latitude</b>	<b>Al</b>	<b>B</b>	<b>Ba</b>	<b>Ca</b>
SMS_L_7.3	7.3	44.5512	-0.006	1.184	0.001	127.708
SMS_L_9.0	9	44.5512	-0.004	2.026	0.003	201.042
SMS_L_11.0	11	44.5512	-0.007	1.441	0.004	181.429
SMS_L_12.0A	12	44.5512	-0.006	2.039	0.003	193.037
SMS_L_12.0B	12	44.5512	0.002	2.106	0.003	118.962
SMS_L_12.0C	12	44.5512	-0.007	1.572	0.006	120.05
SMS_L_12.0	12	44.5512	-0.006	1.726	0.009	143.909
SMS_L_12.0D	12	44.5512	-0.006	1.529	0.005	130.509
SMS_L_12.0E	12	44.5512	-0.004	1.899	0.002	139.699
SMS_L_12.0F	12	44.5512	-0.007	0.909	0.004	143.081
SMS_L_13.2	13.2	44.5512	-0.006	1.952	0.006	141.994
SMS_L_16.5	16.5	44.5512	-0.007	1.491	0.003	121.129
HAR_L_7.7	7.7	44.3667	0	1.305	0.002	114.289
HAR_L_8.4A	8.4	44.3667	-0.011	1.435	0.003	175.818
HAR_L_8.4B	8.4	44.3667	-0.009	1.175	0.003	177.065
HAR_L_8.4C	8.4	44.3667	-0.011	1.468	0.003	188.856
HAR_L_8.4	8.4	44.3667	-0.008	1.386	0.002	149.951
HAR_L_8.4D	8.4	44.3667	-0.005	1.805	0.002	147.9
HAR_L_8.4E	8.4	44.3667	-0.008	1.317	0.002	173.149
HAR_L_8.4F	8.4	44.3667	-0.002	2.058	0.002	123.72
HAR_L_9.0	9	44.3667	-0.004	1.977	0.003	156.282
HAR_L_10.0A	10	44.3667	-0.005	1.316	0.005	180.051
HAR_L_10.0B	10	44.3667	-0.007	1.528	0.01	191.358
HAR_L_10.0C	10	44.3667	-0.007	1.679	0.004	167.271
HAR_L_10.0	10	44.3667	-0.005	1.863	0.004	183.114
HAR_L_10.0D	10	44.3667	-0.008	1.435	0.005	167.768
HAR_L_10.0E	10	44.3667	-0.007	1.644	0.004	144.142
HAR_L_10.0F	10	44.3667	-0.009	1.433	0.008	185.819

<b>Sample</b>	<b>Ca</b>	<b>Cd</b>	<b>Co</b>	<b>Cr</b>	<b>Cu</b>	<b>Fe</b>	<b>K</b>
DI_blank	0.001	0	0	0.001	0	0.009	0.173
GSRN_L_26.0	97.794	0	0	0.001	-0.001	0.007	0.349
GSR_L_1.1	112.763	0	0	0	0	0.005	0.353
GSR_L_8.2	132.871	0	0	0.001	0	0.004	0.318
GSR_L_40.0	156.012	0	0	0.001	-0.001	0.006	0.348
1138_L_8.9	140.588	0	0	0.001	-0.002	0.003	0.326
TrC_L_6.3	142.262	0	0	0	-0.002	0.005	0.556
TrC_L_7.2	137.325	0	0	0.001	0	0.005	0.296
TrC_L_10.0	191.127	0	0	0.001	-0.001	0.079	0.425
TrC_L_10.8	111.4	0	0	0	-0.001	0.005	0.234

Sample	Ca	Cd	Co	Cr	Cu	Fe	K
TrC_L_13.0	136.205	0	0	0.001	0	0.005	0.387
TrC_L_14.0	124.045	0	0	0	0.001	0.004	0.38
TrC_L_17.4	154.231	0	0	0.001	0	0.003	0.387
TrC_L_19.7	177.959	0	0	0	-0.001	0.001	0.191
TrC_L_21.5	126.896	0	0.001	0.001	-0.002	0.006	0.44
TrC_L_25.5	150.591	0	-0.001	0	-0.001	0.008	0.439
TrC_L_30.0	129.554	0	0	0.001	-0.001	0.005	0.439
TrC_L_36.0	138.306	0	0	0	-0.001	0.006	0.478
TrC_L_49.0	137.963	0	0	0.001	-0.001	0.005	0.431
SM_L_1.0	110.279	0	0	0.001	-0.001	0.007	0.257
SMS_L_1.7	162.332	0.001	0	0.001	0.002	0.006	0.447
SMS_L_4.2A	100.832	0	0	0.001	0.002	0.01	0.424
SMS_L_4.2B	140.618	0	0	0	0.002	0.006	0.455
SMS_L_4.2C	104.556	0	0	0.001	0.001	0.005	0.469
SMS_L_4.2	173.661	0	0	0.001	0.001	0.009	0.317
SMS_L_4.2D	146.256	0	0	0.001	0.001	0.005	0.379
SMS_L_4.2E	160.837	0	0	0	0	0.006	0.52
SMS_L_4.2F	93.961	0	0	0	0.001	0.008	0.475
SMS_L_5.6	113.496	0	0	0	0	0.005	0.543
SMS_L_6.3	122.357	0	0	0	-0.001	0.005	0.319
SMS_L_6.7	91.289	0	-0.001	0.002	0.002	0.006	0.184
SMS_L_7.3	127.708	0	0	0.001	0.001	0.007	0.215
SMS_L_9.0	201.042	0	-0.001	0.001	-0.001	0.002	0.41
SMS_L_11.0	181.429	0	0.001	0.001	-0.001	0.004	0.361
SMS_L_12.0A	193.037	0	-0.001	0.001	-0.001	0.006	0.338
SMS_L_12.0B	118.962	0	0	0.001	-0.001	0.005	0.325
SMS_L_12.0C	120.05	0	-0.001	0.001	-0.001	0.006	0.361
SMS_L_12.0	143.909	0	-0.001	0.001	0	0.005	0.449
SMS_L_12.0D	130.509	0	-0.001	0.001	0	0.006	0.404
SMS_L_12.0E	139.699	0	-0.001	0.001	-0.001	0.005	0.407
SMS_L_12.0F	143.081	0	0	0.002	0	0.004	0.326
SMS_L_13.2	141.994	0	0	0.002	0	0.006	0.268
SMS_L_16.5	121.129	0	-0.001	0.001	0	0.007	0.369
HAR_L_7.7	114.289	0	0	0.001	-0.001	0.009	0.269
HAR_L_8.4A	175.818	0	-0.001	0.001	-0.001	0.009	0.348
HAR_L_8.4B	177.065	-0.001	0	0.001	-0.003	0.005	0.33
HAR_L_8.4C	188.856	-0.001	-0.001	0.001	-0.002	0.005	0.399
HAR_L_8.4	149.951	0	-0.001	0.001	-0.002	0.007	0.363
HAR_L_8.4D	147.9	0	-0.001	0.001	-0.002	0.006	0.353
HAR_L_8.4E	173.149	0	-0.001	0.001	-0.002	0.005	0.272

<b>Sample</b>	<b>Ca</b>	<b>Cd</b>	<b>Co</b>	<b>Cr</b>	<b>Cu</b>	<b>Fe</b>	<b>K</b>
HAR_L_8.4F	123.72	0	-0.001	0.001	-0.002	0.006	0.328
HAR_L_9.0	156.282	0	-0.001	0.002	-0.001	0.007	0.389
HAR_L_10.0A	180.051	0	-0.001	0.001	-0.002	0.005	0.424
HAR_L_10.0B	191.358	0	-0.001	0.002	-0.001	0.013	0.438
HAR_L_10.0C	167.271	0	-0.001	0.001	-0.002	0.006	0.454
HAR_L_10.0	183.114	0	-0.001	0.001	-0.003	0.008	0.375
HAR_L_10.0D	167.768	0	-0.001	0.001	-0.003	0.008	0.377
HAR_L_10.0E	144.142	0	-0.001	0.002	-0.002	0.005	0.289
HAR_L_10.0F	185.819	0	0	0.001	-0.003	0.005	0.48

<b>Sample</b>	<b>Mg</b>	<b>Mn</b>	<b>Mo</b>	<b>Na</b>	<b>Ni</b>	<b>P</b>	<b>Pb</b>
DI_blank	0.001	0	0.027	2.066	0.001	-0.03	-0.003
GSRN_L_26.0	0.052	0.001	0.019	2.078	0.002	-0.006	0.001
GSR_L_1.1	0.036	0.001	0.011	2.124	0.002	-0.002	-0.001
GSR_L_8.2	0.036	0.001	0.008	1.827	0.002	-0.003	0.005
GSR_L_40.0	0.041	0.001	0.005	2.401	0.002	0.003	0.003
1138_L_8.9	0.104	0.001	0.005	1.939	0.001	-0.004	0.005
TrC_L_6.3	0.051	0.001	0.003	2.783	0.002	-0.01	-0.001
TrC_L_7.2	0.033	0.001	0.003	1.6	0.002	-0.012	-0.003
TrC_L_10.0	0.151	0.003	0.002	1.831	0.003	0	0.004
TrC_L_10.8	0.029	0.001	0.003	1.59	0.002	-0.015	0.004
TrC_L_13.0	0.054	0.001	0.008	2.034	0.002	-0.022	0.004
TrC_L_14.0	0.059	0.002	0.007	2.194	0.002	0.02	0.004
TrC_L_17.4	0.063	0.001	0.006	3.242	0.003	-0.018	0.002
TrC_L_19.7	0.078	0.001	0.005	1.212	0.003	-0.02	0.004
TrC_L_21.5	0.052	0.001	0.004	3.363	0.002	-0.016	0.001
TrC_L_25.5	0.058	0.003	0.003	3.387	0.003	-0.011	0.006
TrC_L_30.0	0.039	0.001	0.002	2.053	0.002	-0.02	0.001
TrC_L_36.0	0.056	0.002	0.002	3.815	0.002	-0.02	0.003
TrC_L_49.0	0.037	0.001	0.001	2.313	0.003	-0.018	0.002
SM_L_1.0	0.028	0.001	0.002	2.185	0.002	-0.021	0.005
SMS_L_1.7	0.064	0.001	0.035	3.375	0.003	-0.028	0.003
SMS_L_4.2A	0.05	0.003	0.022	2.506	0.004	-0.028	0.001
SMS_L_4.2B	0.05	0.001	0.016	2.017	0.003	-0.031	0
SMS_L_4.2C	0.037	0.001	0.011	2.08	0.002	-0.028	-0.002
SMS_L_4.2	0.055	0.001	0.011	3.062	0.003	-0.018	-0.002
SMS_L_4.2D	0.058	0.001	0.008	2.498	0.003	-0.03	0.002
SMS_L_4.2E	0.052	0.001	0.006	2.56	0.002	-0.025	0.001
SMS_L_4.2F	0.05	0.001	0.004	3.249	0.002	-0.04	0.001
SMS_L_5.6	0.06	0.001	0.006	2.525	0.003	-0.023	0.002

<b>Sample</b>	<b>Mg</b>	<b>Mn</b>	<b>Mo</b>	<b>Na</b>	<b>Ni</b>	<b>P</b>	<b>Pb</b>
SMS_L_6.3	0.076	0.001	0.004	1.84	0.003	-0.034	0.001
SMS_L_6.7	0.028	0	0.005	1.565	0.001	0.029	0.002
SMS_L_7.3	0.032	0	0.002	1.846	0.001	0.038	0.007
SMS_L_9.0	0.088	0.001	0.003	3.556	0.001	0.042	0.007
SMS_L_11.0	0.066	0.001	0.001	2.167	0.001	0.031	0.006
SMS_L_12.0A	0.054	0.001	0	3.513	0.002	0.04	0.006
SMS_L_12.0B	0.051	0.001	0	3.694	0	0.024	0.006
SMS_L_12.0C	0.043	0.001	0	2.294	0.001	0.027	0.006
SMS_L_12.0	0.074	0.001	0	2.666	0.001	0.031	0.005
SMS_L_12.0D	0.044	0.001	0	2.299	0.001	0.032	0.004
SMS_L_12.0E	0.044	0.001	0.001	3.257	0.001	0.033	0.003
SMS_L_12.0F	0.032	0.001	0.006	1.43	0.001	0.025	0.005
SMS_L_13.2	0.05	0.001	0.003	3.19	0.001	0.022	0.005
SMS_L_16.5	0.036	0.001	0.003	2.315	0	0.024	0.006
HAR_L_7.7	0.034	0.001	0.002	2.276	0.001	0.075	0.001
HAR_L_8.4A	0.049	0.001	0	2.143	0.001	0.029	0.003
HAR_L_8.4B	0.058	0.001	0	1.759	0.001	0.031	0.004
HAR_L_8.4C	0.049	0.001	0.001	2.157	0.001	0.034	0.005
HAR_L_8.4	0.043	0.001	0	2.138	0.001	0.029	0.003
HAR_L_8.4D	0.081	0.003	0.001	3.29	0.002	0.029	0.007
HAR_L_8.4E	0.058	0.001	-0.001	2.121	0.002	0.033	0.006
HAR_L_8.4F	0.041	0.001	0	3.567	0.001	0.077	0.008
HAR_L_9.0	0.044	0.001	0.031	3.529	0.001	0.084	0.004
HAR_L_10.0A	0.06	0.001	0.017	2.115	0.002	0.077	0.006
HAR_L_10.0B	0.123	0.001	0.01	2.257	0.001	0.031	0.005
HAR_L_10.0C	0.062	0.001	0.008	2.738	0.002	0.071	0.005
HAR_L_10.0	0.076	0.001	0.007	3.294	0.001	0.081	0.012
HAR_L_10.0D	0.057	0.001	0.005	2.323	0.001	0.029	0.008
HAR_L_10.0E	0.051	0.001	0.005	2.49	0	0.077	0.005
HAR_L_10.0F	0.074	0.001	0.003	2.242	0.001	0.074	0.004

<b>Sample</b>	<b>Si</b>	<b>Sr</b>	<b>Zn</b>
DI_blank	7.06	0	0
GSRN_L_26.0	9.415	0.245	0.027
GSR_L_1.1	9.039	0.322	0.006
GSR_L_8.2	8.867	0.295	0.003
GSR_L_40.0	9.955	0.416	0.002
1138_L_8.9	9.003	0.418	0.009
TrC_L_6.3	10.176	0.359	0.004
TrC_L_7.2	8.422	0.326	0.007

Sample	Si	Sr	Zn
TrC_L_10.0	9.293	0.352	0.006
TrC_L_10.8	8.43	0.295	0.003
TrC_L_13.0	8.943	0.384	0.003
TrC_L_14.0	9.526	0.342	0.004
TrC_L_17.4	10.826	0.658	0.002
TrC_L_19.7	7.721	0.766	0.003
TrC_L_21.5	10.519	0.383	0.055
TrC_L_25.5	10.818	0.512	0.01
TrC_L_30.0	9.285	0.442	0.006
TrC_L_36.0	10.952	0.595	0.008
TrC_L_49.0	9.245	0.594	0.022
SM_L_1.0	8.95	0.391	0.002
SMS_L_1.7	11.004	0.366	0.002
SMS_L_4.2A	9.563	0.364	0.003
SMS_L_4.2B	9.339	0.433	0.006
SMS_L_4.2C	8.807	0.252	0.003
SMS_L_4.2	10.732	0.466	0.005
SMS_L_4.2D	9.97	0.453	0.001
SMS_L_4.2E	10.052	0.48	0.002
SMS_L_4.2F	10.396	0.243	0.006
SMS_L_5.6	9.882	0.3	0.004
SMS_L_6.3	8.526	0.466	0.005
SMS_L_6.7	8.421	0.109	0.002
SMS_L_7.3	9.246	0.325	0.003
SMS_L_9.0	11.41	0.443	0.001
SMS_L_11.0	9.751	0.551	0.003
SMS_L_12.0A	11.398	0.439	0.003
SMS_L_12.0B	11.022	0.319	0.002
SMS_L_12.0C	9.907	0.325	0.001
SMS_L_12.0	10.414	0.466	0.001
SMS_L_12.0D	9.657	0.363	0.002
SMS_L_12.0E	10.744	0.315	0.002
SMS_L_12.0F	8.072	0.372	0.005
SMS_L_13.2	11.133	0.484	0.001
SMS_L_16.5	9.775	0.288	0.003
HAR_L_7.7	9.504	0.381	0.004
HAR_L_8.4A	9.734	0.73	0.002
HAR_L_8.4B	9.274	0.535	0.001
HAR_L_8.4C	10.005	0.578	0
HAR_L_8.4	9.918	0.414	0.003

Sample	Si	Sr	Zn
HAR_L_8.4D	10.69	0.438	0.001
HAR_L_8.4E	9.393	0.494	0.003
HAR_L_8.4F	11.084	0.317	0.001
HAR_L_9.0	10.962	0.35	0.002
HAR_L_10.0A	9.688	0.535	0.002
HAR_L_10.0B	10.164	0.648	0.003
HAR_L_10.0C	10.292	0.51	0.004
HAR_L_10.0	11.028	0.491	0
HAR_L_10.0D	9.824	0.609	0.002
HAR_L_10.0E	10.158	0.459	0.009
HAR_L_10.0F	9.758	0.717	0.003